



# Functional expression of TMEM16A in taste bud cells

Domenico M. Guarascio<sup>1</sup>, Kevin Y. Gonzalez-Velandia<sup>1</sup>, Andres Hernandez-Clavijo<sup>1</sup> , Anna Menini<sup>1</sup> and Simone Pifferi<sup>1,2</sup> 

<sup>1</sup>Neurobiology Group, SISSA, Scuola Internazionale Superiore di Studi Avanzati, Trieste, 34136, Italy

<sup>2</sup>Department of Experimental and Clinical Medicine, Università Politecnica delle Marche, Ancona, 60126, Italy

Edited by: Don Bers and Robert Harvey

The peer review history is available in the Supporting Information section of this article (<https://doi.org/10.1113/JP281645#support-information-section>).

## Key points

- Taste transduction occurs in taste buds in the tongue epithelium.
- The Ca<sup>2+</sup>-activated Cl<sup>-</sup> channels TMEM16A and TMEM16B play relevant physiological roles in several sensory systems.
- Here, we report that TMEM16A, but not TMEM16B, is expressed in the apical part of taste buds.
- Large Ca<sup>2+</sup>-activated Cl<sup>-</sup> currents blocked by Ani-9, a selective inhibitor of TMEM16A, are measured in type I taste cells but not in type II or III taste cells.
- ATP indirectly activates Ca<sup>2+</sup>-activated Cl<sup>-</sup> currents in type I cells through TMEM16A channels.
- These results indicate that TMEM16A is functional in type I taste cells and contribute to understanding the largely unknown physiological roles of these cells.

**Abstract** The Ca<sup>2+</sup>-activated Cl<sup>-</sup> channels TMEM16A and TMEM16B have relevant roles in many physiological processes including neuronal excitability and regulation of Cl<sup>-</sup> homeostasis. Here, we examined the presence of Ca<sup>2+</sup>-activated Cl<sup>-</sup> channels in taste cells of mouse vallate papillae by using immunohistochemistry and electrophysiological recordings. By using immunohistochemistry we showed that only TMEM16A, and not TMEM16B, was expressed in taste bud cells where it largely co-localized with the inwardly rectifying K<sup>+</sup> channel KCNJ1 in the apical part of type I cells. By using whole-cell patch-clamp recordings in isolated cells from taste buds, we measured an average current of  $-1083$  pA at  $-100$  mV in  $1.5$   $\mu$ M Ca<sup>2+</sup> and symmetrical Cl<sup>-</sup> in type I cells. Ion substitution experiments and blockage by Ani-9, a specific TMEM16A channel blocker, indicated that Ca<sup>2+</sup>-activated anionic currents through TMEM16A channels. We did not detect any Ca<sup>2+</sup>-activated Cl<sup>-</sup> currents in type II or III taste cells. ATP is released by type II cells in response to various tastants and reaches type I cells where it is hydrolysed by ecto-ATPases. Type I cells also express P2Y purinergic receptors and stimulation of type I cells with extracellular ATP produced large Ca<sup>2+</sup>-activated Cl<sup>-</sup> currents blocked by Ani-9, indicating a possible role of TMEM16A in ATP-mediated signalling. These results provide a definitive demonstration that TMEM16A-mediated currents are functional

Domenico M. Guarascio got his Master degree in Biology of Health at the University of Bologna (Italy). In 2016 he started his Ph.D. in neurobiology, under the supervision of Prof. Anna Menini and Prof. Simone Pifferi, at International School of Advanced Studies in Trieste (IT). Currently he is finishing his fourth year of Ph.D. with a thesis about the localization and the functional expression of the TMEM16A, Calcium-activated Chloride Channel (CaCC) in mouse taste bud cells.



in type I taste cells and provide a foundation for future studies investigating physiological roles for these often-neglected taste cells.

(Received 8 May 2021; accepted after revision 4 June 2021; first published online 5 June 2021)

**Corresponding authors** A. Hernandez-Clavijo and A. Menini: Neurobiology Group, SISSA, Scuola Internazionale Superiore di Studi Avanzati, 34136 Trieste, Italy. Email: ahernand@sisssa.it and menini@sisssa.it

S. Pifferi: Department of Experimental and Clinical Medicine, Università Politecnica delle Marche, Via Tronto 10A, Ancona 60126, Italy. Email: s.pifferi@staff.univpm.it

## Introduction

In vertebrates, the process of taste transduction occurs in cells of taste buds that are mainly located in the tongue epithelium. Taste buds are onion-shaped clusters of about 50–100 elongated epithelial cells that extend from the basal lamina to the surface of the tongue, where a pore allows the apical part of taste cells to directly contact chemicals dissolved in the mouth saliva. Taste buds also contain basal cells that will form new taste cells. In several species, at least three main types of elongated taste cells have been identified and named type I, II or III. These cell types can be distinguished based on their ultrastructural morphology, expression of specific proteins and functional properties. Type II and type III cells express taste receptors and respond to tastants, while type I cells mainly have glial-like functions. Type I cells have also been suggested to be involved in salt transduction because they express amiloride-sensitive  $\text{Na}^+$  channels (Vandenbeuch *et al.* 2008; Roper & Chaudhari, 2017; Baumer-Harrison *et al.* 2020; Yang *et al.* 2020), but a recent study demonstrated that amiloride-sensitive salt taste is transmitted to the nervous system by a unique cell type that expresses the ATP release channel CALHM1/3 and voltage-gated  $\text{Na}^+$  channels, neither of which are found in type I taste cells (Nomura *et al.* 2020).

Type II cells express G protein-coupled receptors for sweet (TAS1R2–TAS1R3), umami (TAS1R1–TAS1R3) or bitter (TAS2Rs) detection and use at least one common transduction cascade that involves the G-protein alpha subunit gustducin (GNAT3), phospholipase-C-beta-2 (PLC $\beta$ 2), inositol-3-phosphate (IP3) and  $\text{Ca}^{2+}$  release from intracellular stores (Zhang *et al.* 2003; Hisatsune *et al.* 2007). The increased intracellular  $\text{Ca}^{2+}$  concentration activates TRPM5 and TRPM4, causing membrane depolarization by  $\text{Na}^+$  entry and release of ATP through voltage-gated CALHM1/CALHM3 channels (Dutta Banik *et al.* 2018; Ma *et al.* 2018).

Type III cells mediate sour detection through the apical ion channel OTOPI1 that allows entry of  $\text{H}^+$  and cell membrane depolarization, which is further amplified by the block of the inwardly rectifier  $\text{K}^+$  channel KCNJ2 by low pH (Ye *et al.* 2016; Tu *et al.* 2018; Teng *et al.* 2019). Type III is the only taste cells that form canonical synapses with afferent nerve fibres.

They express the presynaptic synaptosomal-associated protein 25 (SNAP25), the glutamic acid decarboxylase 67 (GAD67) and voltage-gated  $\text{Ca}^{2+}$  channels, which trigger the release of neurotransmitters (Yang *et al.* 2000; DeFazio *et al.* 2006; Tomchik *et al.* 2007; Huang *et al.* 2008; Vandenbeuch *et al.* 2010).

Type I cells are called ‘glial-like’ cells and are mainly considered to have a supporting role in the taste buds. These cells have projections that wrap around other cells and express proteins involved in removing neurotransmitters, such as the ectonucleotidase NTPDase2 (encoded by *Entpd2*) and the glutamate transporter GLAST (Lawton *et al.* 2000; Bartel *et al.* 2006). Moreover, the inwardly rectifier  $\text{K}^+$  channel KCNJ1 (also named  $\text{K}_{\text{ir}}1.1$  or renal outer medullary K, ROMK) is expressed at the apical tips of type I cells and may be involved in  $\text{K}^+$  homeostasis (Dvoryanchikov *et al.* 2009).

The three cell types can also be identified by their electrophysiological fingerprint. Indeed, by using voltage-clamp whole-cell recordings in pseudo-physiological solutions, type I cells are characterized by the presence of voltage-gated outward  $\text{K}^+$  currents and no inward currents, type II cells by voltage-gated inward  $\text{Na}^+$  currents and voltage-gated outward non-selective currents, and type III cells by voltage-gated inward  $\text{Na}^+$  and  $\text{Ca}^{2+}$  currents and by voltage gated-outward  $\text{K}^+$  currents (Medler *et al.* 2003; Clapp *et al.* 2006; Romanov & Kolesnikov, 2006; Romanov *et al.* 2007; Taruno *et al.* 2013).

Multiple chloride conductances, including  $\text{Ca}^{2+}$ -dependent  $\text{Cl}^-$  currents, have been recorded in some taste cells (McBride & Roper, 1991; Taylor & Roper, 1994; Wladkowski *et al.* 1998; Herness & Sun, 1999; Kim *et al.* 2000; Cherkashin *et al.* 2016). Kim *et al.* (2000) clearly demonstrated that a subpopulation of unidentified taste cells had  $\text{Ca}^{2+}$ -activated  $\text{Cl}^-$  currents and that extracellular ATP could indirectly activate these channels by intracellular  $\text{Ca}^{2+}$  increase through activation of P2Y receptors.  $\text{Ca}^{2+}$ -activated  $\text{Cl}^-$  channels are encoded by two proteins of the TMEM16 family, TMEM16A and TMEM16B (also named Ano1 and Ano2, respectively). They share several electrophysiological properties such as ionic permeability and voltage dependence but can be functionally distinguished by different  $\text{Ca}^{2+}$  sensitivity and pharmacological profile (Caputo *et al.* 2008;

Schroeder *et al.* 2008; Yang *et al.* 2008; Stephan *et al.* 2009; Stöhr *et al.* 2009; Pifferi *et al.* 2009a; Scudieri *et al.* 2012; Pedemonte & Galietta, 2014). Cherkashin *et al.* (2016) confirmed and extended previous results from Kim *et al.* (2000) showing that the population of taste cells generating Ca<sup>2+</sup>-activated Cl<sup>-</sup> currents in response to P2Y agonists largely consisted of type I cells, but that also some type II cells exhibited small Ca<sup>2+</sup>-activated Cl<sup>-</sup> currents. They indicated that TMEM16B was functional in type I cells, TMEM16A and TMEM16B produced small currents in type II cells, while type III cells did not exhibit any Ca<sup>2+</sup>-activated Cl<sup>-</sup> current.

Here, by taking advantage of *Tmem16a* and *Tmem16b* knockout (KO) mice models (Rock *et al.* 2008; Zhang *et al.* 2017) and of a recently discovered specific blocker of TMEM16A, Ani-9 (Seo *et al.* 2016), we re-examined the functional expression of the two Ca<sup>2+</sup>-dependent Cl<sup>-</sup> channels of the TMEM16 family in taste cells of vallate papillae by using electrophysiological recordings and immunohistochemistry. Surprisingly, we found that only TMEM16A, and not TMEM16B, is expressed in taste buds. In particular, TMEM16A is largely colocalized with the inwardly rectifier K<sup>+</sup> channel KCNJ1 at the apical portion of type I cells. Moreover, by using patch-clamp whole-cell recordings, we functionally measured TMEM16A-mediated currents only in type I and not in type II cells. We then investigated whether TMEM16A-mediated currents in type I cells could be activated by extracellular ATP, a well-known transmitter released by type II cells in taste buds and found that ATP induced Ca<sup>2+</sup>-activated Cl<sup>-</sup> currents that were blocked by Ani-9, further confirming that they were due to TMEM16A channels. We conclude that TMEM16A, but not TMEM16B, plays a role in taste buds.

Although type I cells make up more than 50% of the cells in each taste bud and are known to have glial-like functions, they have often been overlooked in favour of studies on type II and III cells. A complete knowledge of the functional ion channels of type I cells will help to understand additional roles that these cells may play in taste buds. Although further studies are required to determine the physiological role of TMEM16A in taste buds, we discuss some possible scenarios.

## Methods

### Animals and ethical approval

Mice were handled according to the guidelines of the Italian Animal Welfare Act (Decreto legislativo 26/2014/) and European Union guidelines on animal research (2010/63) under a protocol approved by the Italian Ministry of Health. Mice had free access to water and food. Every effort was made to reduce the number of animals used. Adult (> 8 weeks) mice were anaesthetized with

CO<sub>2</sub> and decapitated before tongue and nose removal. Mice were transferred to a cage (8 × 10 × 12 cm, height/width/length) and 100% CO<sub>2</sub> was slowly injected into the cage until the animal stopped breathing and no longer displayed pedal reflex (near 3 min, gas flow rate was ~20% of chamber volume per minute). Young mice, postnatal days 8–10 (P8–P10), were decapitated before tongue removal. Experiments were performed on tissues from both male and female C57BL/6, GAD67-GFP (Oliva *et al.* 2000), *Tmem16a* KO (Rock *et al.* 2008) or mCherry *Tmem16b* KO mice (Zhang *et al.* 2017). *Tmem16a* KO and wild-type (WT) littermates were obtained by breeding heterozygous mice. mCherry *Tmem16b* KO mice were kindly provided by Dr Lily Jan (University of California, San Francisco, USA, Zhang *et al.* 2017). The generated *Tmem16b*-deficient mice were engineered by inserting mCherry sequence with a farnesylation signal at the C-terminus (mCherry-F) in frame with the alternative start ATG codon in the third exon of *Tmem16b*, and therefore membrane-associated mCherry marks cells that normally express *Tmem16b* (see fig. S2C of Zhang *et al.* 2017).

### Tissue preparation

The epithelium containing the taste papillae was peeled using an enzymatic–mechanical dissociation protocol slightly modified from those previously reported (Béhé *et al.* 1990; Bigiani, 2001; Cherkashin *et al.* 2016). Once removed, the tongue was placed in a Sylgard Petri dish filled with a standard mammalian Ringer solution containing (in mM): 140 NaCl, 5 KCl, 2 CaCl<sub>2</sub>, 1 MgCl<sub>2</sub>, 10 HEPES, 10 glucose, pH 7.4, with NaOH. Using an insulin syringe, 0.5 ml Ringer solution containing 2 mg ml<sup>-1</sup> dispase II (D4693, Sigma, St Louis, MO, USA), 0.2 mg ml<sup>-1</sup> elastase (E0127, Sigma) and 0.7 mg ml<sup>-1</sup> collagenase B (C9891, Sigma) was injected under the epithelium. The syringe needle was carefully inserted from the posterior to the most anterior part of the tongue. Injection of the enzymatic solution was performed while the needle was gently withdrawn to allow the solution to reach the entire epithelium. After 30 min of incubation, the epithelium was peeled off from the underlying muscle and the vallate papilla and taste cells were isolated as described in the following sections.

### RT-PCR

The vallate papilla was cut from the peeled tongue epithelium and directly placed in the lysis buffer of the mRNA isolation kit (S1550S, New England Biolabs, Ipswich, MA, USA). The olfactory epithelium was isolated as previously described (Pifferi *et al.* 2006; Sagheddu *et al.* 2010). The olfactory turbinates were exposed by bisecting the head along the midline, the epithelium was

carefully removed from turbinates, septum and the roof of the nasal cavity and placed directly in the lysis buffer of the mRNA isolation kit. Vallate papillae mRNA was extracted from four adult C57BL/6 mice and olfactory epithelium mRNA was extracted from two adult C57BL/6 mice. The mRNA isolation kit was used with Oligo d(T)<sub>25</sub> magnetic beads for mRNA isolation. After extraction, mRNA was further incubated with DNAase I (M0303S, New England Biolabs) to remove any residual genomic DNA. cDNA was synthesized using the SMARTER cDNA synthesis kit from 25 ng of mRNA (634860, Takara, Shiga, Japan).

PCR was performed in a thermocycler (ThermoCycler2720, Life Technologies, Carlsbad, CA, USA) using Phusion HS II High-Fidelity DNA Polymerase (F549S, ThermoFisher Scientific, Waltham, MA, USA), 0.2 mM for each dNTPs (N0447S, New England Biolabs) and 200 pmol forward/reverse target-specific primers. Cycling parameters were: an initial denaturation step (98°C, 2 min) followed by 38 cycles, each of these cycles including a denaturation step (98°C, 10 s), a primer annealing step (62–64°C, 30 s) and an extension step (72°C, 30 s) step. The reaction was completed by a final extension step at 72°C for 5 min.

The following primer sequences were used to amplify target DNAs: *Gapdh* fwd 5'-TGCTGAGTATGTCGTGGAGTCT-3' rev 5'-TGCTGTAGCCGATTCATTGTC-3' (T<sub>m</sub> = 64°C; 691 bp; GenBank accession no. NM\_008084.3); *Olfir73* fwd 5'-GCTGGTATTGGGATCCTATGCTT-3' rev 5'-CGTCCACTTGCTGACTTCATCTT-3' (T<sub>m</sub> = 62°C; 272 bp; GenBank accession no. NM\_054090.1); *Tmem16a* fwd 5'-ATGAAGCCAGAGTCTTAGAGAAGT-3' rev 5'-AAACTTCATCCAGCAGAATGAT-3' (T<sub>m</sub> = 62°C; 296 bp; GenBank accession no. NM\_178642.6); *Tmem16b* fwd 5'-ATGCACTTTCACGACAACCA-3' rev 5'-GCCCAGCAGCCATCAGGTTG-3' (T<sub>m</sub> = 62°C; 243 bp; GenBank accession no. NM\_001364563.1); *Entpd2* fwd 5'-CTCAAGTATGGCATCGTTCTGG-3' rev 5'-CAGAGACGAGGTCACGACAGAG-3' (T<sub>m</sub> = 62°C; 834 bp; GenBank accession no. NM\_009849.2); *Plcβ2* fwd 5'-TGGAGGTGACAGCTTATGAGGA-3' rev 5'-GGTTGGCAAGGGCTACTGTAAG-3' (T<sub>m</sub> = 62°C; 842 bp; GenBank accession no. NM\_001290790.1); *Snap25* fwd 5'-TGGCATCAGGACTTTGGTTATG-3' rev 5'-GCATCTTTGTTGCACGTTGGT-3' (T<sub>m</sub> = 62°C; 481 bp; GenBank accession no. NM\_001355254.1). The products were visualized following agarose gel electrophoresis (1.5%) and DNA was stained with Midori Green Advance (MG04, Nippon Genetics, Düren, Germany).

### Immunohistochemistry

Immunohistochemistry was performed on tongue sections containing the vallate papilla and on olfactory

epithelium sections. The dissected tongues were directly fixed in 4% paraformaldehyde in PBS, pH 7.4, for 3–4 h at 4°C. For nose isolation, the lower jaw, the posterior part of the brain and the skinhead were removed. The remaining head, containing the nasal cavity, was fixed in 4% paraformaldehyde in PBS, pH 7.4, for 4–5 h at 4°C and then decalcified in 0.5 M EDTA, pH 8, for 2 days, as previously described (Pifferi *et al.* 2006, 2009b; Maurya & Menini, 2014; Maurya *et al.* 2015; Henriques *et al.* 2019). For cryoprotection, tongue and olfactory tissues were equilibrated overnight in 30% (w/v) sucrose in PBS at 4°C. Tissues were frozen in optimal cutting temperature compound (Bio-Optica, Milan, Italy) and stored at –80°C before sectioning with a cryostat. Coronal sections (14–16 μm thick) were cut with a cryostat and mounted on Superfrost Plus Adhesion Microscope Slides (ThermoFisher Scientific). Sections were air-dried for 3 h and stored at –80°C for further use. For antigen retrieval, sections were kept in SDS 0.5% (w/v) in PBS for 15 min at room temperature. After pre-treatment, sections were incubated in blocking solution [5% (v/v) FBS or donkey serum and 0.3% (v/v) Triton X-100 in PBS] for 2 h, and then with the primary antibody (diluted in the blocking solution) overnight at 4°C. Slices were then rinsed with PBS and incubated with the chosen fluorophore-conjugated secondary antibody diluted in PBS-T (0.1% Tween 20 in PBS) for 2 h at room temperature. After washing with PBS-T, sections were treated with DAPI (0.2 μg/ml) for 30 min, washed with PBS-T, and mounted with Vectashield (Vector Laboratories, Burlingame, CA, USA) or Fluoromount-G (ThermoFisher).

The following primary antibodies (dilution; catalogue number, company) were used: polyclonal rabbit anti-TMEM16A (1:100; ab53212, Abcam, Cambridge, MA, USA), polyclonal goat anti-TMEM16A (1:50; sc-69343, Santa Cruz Biotechnology, Santa Cruz, CA, USA), polyclonal rabbit anti-TMEM16B (1:200; 20 647-1-P; Proteintech, Rosemont, IL, USA), polyclonal rabbit anti-NTPDase2 (1:500; mN2-36LI6, from J. Sévigny at Centre de Recherche du CHU de Québec, Université Laval, Quebec <http://ectonucleotidases-ab.com>), polyclonal rabbit anti-KCNJ (1:500; APC-001, Alomone Labs, Jerusalem, Israel), polyclonal goat anti-GNAT3 (1:1000; OAEB00418, Aviva Systems Biology, San Diego, CA, USA), polyclonal rabbit anti-PLCβ2 (1:200; sc-206, Santa Cruz Biotechnology), polyclonal chicken anti-GFP (1:200; GTX13970, GeneTex, Irvine, CA, USA), polyclonal rabbit anti-RFP antibody (1:500, 600-401-379, Rockland). The following secondary antibodies were used: donkey anti-rabbit Alexa Fluor Plus 594 (1:500; A32754, Life Technologies), donkey anti-goat Alexa Fluor 488 (1:500; A11055, Life Technologies), donkey anti-rabbit Alexa Fluor 488 (1:500; A21206, Life Technologies), donkey anti-goat Alexa Fluor Plus 647 (1:500; A32849, Life

Technologies), goat anti-chicken Alexa Fluor 488 (1:500, A-11 039, Invitrogen, Carlsbad, CA, USA).

Immunofluorescence was visualized with a confocal laser scanning microscope (A1R or C1, Nikon, Tokyo, Japan). Images were acquired using NIS-Elements Nikon software at  $1024 \times 1024$  pixels resolution and analysed with ImageJ software (National Institute of Health, Bethesda, MD, USA). Control experiments, excluding primary antibodies, were performed for each immunolocalization experiment and gave no signal. In addition, negative control experiments for the polyclonal rabbit anti-TMEM16A (Fig. 2D) and polyclonal goat anti-TMEM16A (not shown) were made in vallate papillae from *Tmem16a* KO mice.

### Electrophysiological recordings from taste bud cells

The peeled tongue epithelium was placed upside-down in a Sylgard Petri dish, in  $\text{Ca}^{2+}$ -free Ringer solution containing (in mM): 140 NaCl, 5 KCl, 1  $\text{MgCl}_2$ , 0.5 EDTA, 10 Hepes, 10 glucose, pH 7.4, with NaOH. After 30 min of incubation, cells were removed from taste buds of the vallate papilla by gentle suction with a flame-polished glass capillary tube with an opening diameter of 40–50  $\mu\text{m}$  and plated in Petri dishes, pre-coated with 5 mM Concanavalin-A (Type V, Sigma, Milan, Italy), for at least 1 h to favour cell adhesion.

Isolated taste cells were continuously perfused with Ringer solution. Cells were viewed with an inverted microscope (IMT-2 or IX70, Olympus), equipped with  $10\times$  and  $40\times$  objectives and an additional  $1.5\times$  auxiliary lens, and identified by their elongated shape. Whole-cell membrane currents were recorded at room temperature (21–24°C) in the voltage-clamp mode, using an Axopatch 200B or a Multiclamp 700B amplifier controlled by Clampex 9 or 10 via a Digidata 1332A (Molecular Devices, Sunnyvale, CA, USA). Patch pipettes were made using borosilicate capillaries (WPI, Sarasota, FL, USA) and pulled with a Narishige PP83 puller (Narishige, Tokyo, Japan). Patch pipettes filled with intracellular solutions had resistances of 2–7 M $\Omega$ . Currents were low-pass filtered at 1 or 5 kHz and sampled at 10 kHz. We used two main intracellular solutions: (i) a KCl-based intracellular solution containing (in mM): 140 KCl, 10 HEDTA, 10 Hepes, pH 7.2, with KOH, and (ii) an *N*-methyl-D-glucamine-Cl (NMDG-Cl)-based solution containing (in mM): 140 NMDG-Cl, 10 HEDTA, 10 Hepes, adjusted to pH 7.2 with NMDG. To measure  $\text{Ca}^{2+}$ -activated currents, 3.209 mM  $\text{CaCl}_2$  was added to the NMDG-Cl solution to obtain the final concentration of 1.5  $\mu\text{M}$  free  $\text{Ca}^{2+}$ , as calculated with the program WinMAXC (C. Patton, Stanford University, Stanford, CA, USA) and previously described in detail (Patton *et al.* 2004; Pifferi *et al.* 2006, 2009a,b). The extracellular

mammalian Ringer solution contained (in mM): 140 NaCl, 5 KCl, 2  $\text{CaCl}_2$ , 1  $\text{MgCl}_2$ , 10 Hepes and 10 glucose, adjusted to pH 7.4 with NaOH. NMDG-Cl extracellular solution contained (in mM): 140 NMDG-Cl, 1  $\text{MgCl}_2$ , 10 Hepes, adjusted to pH 7.4 with NMDG. For ion selectivity experiments, extracellular NMDG-Cl was replaced by NMDG-methanesulfonate (NMDG-MeS). Ani-9 was prepared in DMSO at 10 mM as a stock solution and diluted in the extracellular solution to the final concentration of 1  $\mu\text{M}$ .  $\text{GdCl}_3$  was prepared as a 1 M stock solution and daily diluted in the extracellular solution to the final concentration of 200  $\mu\text{M}$ .

For recordings of ATP-activated currents, the patch pipette solution contained (in mM): 140 NMDG-Cl, 2 HEDTA, 10 Hepes, adjusted to pH 7.2 with NMDG and no added  $\text{Ca}^{2+}$ . ATP at 50  $\mu\text{M}$  was added to the extracellular Ringer solution on the day of the experiment. For ion selectivity experiments, NaCl in the extracellular Ringer solution was replaced by equimolar sodium gluconate. *I-V* relationships were measured using a ramp protocol from  $-70$  to  $+100$  mV at 0.85 mV  $\text{ms}^{-1}$ .

Extracellular solutions were exchanged through a three-barrel square glass (3SG700-5, Warner Instruments, Hamden, CT, USA) using the gravity-driven perfusion system Fast-Step SF-77B (Warner Instruments). Different solutions were flowing side by side in each glass pipe and a stepper motor moved different pipes, and therefore different solution, in front of the cell. The time course of solution exchange was about 50 ms (see Fig. 9A).

The bath was grounded through a 3 M KCl agar bridge connected to an Ag/AgCl reference electrode. Membrane potentials were not corrected for liquid junction potentials whose values were less than 7 mV as calculated using the Clampex's Junction Potential Calculator (based on Barry, 1994).

Chemicals, unless otherwise stated, were purchased from Sigma.

### Electrophysiological recordings from HEK-293 cells

HEK-293 cells were grown in medium composed of DMEM (Gibco, Italy) supplemented with 10% FBS (Sigma, Italy), 100 IU  $\text{ml}^{-1}$  penicillin and 100  $\mu\text{g ml}^{-1}$  streptomycin (Sigma, Italy) at 37°C in a humidified atmosphere of 5%  $\text{CO}_2$ . pEGFP-N1 plasmid containing the cDNA of mouse TMEM16A (version ac, as in Ferrera *et al.* 2009) was provided by Professor Criss Hartzell (Emory University, USA). HEK-293 cells were transfected with 2  $\mu\text{g}$  of plasmid using the transfection reagent XtremeGENE (Roche Diagnostic, Indianapolis, IN, USA). Twenty-four hours after transfection, the cells were subcultured in 35-mm Petri dishes at a lower density. Electrophysiological recordings were performed between 48 and 72 h after transfection as previously described

(Pifferi *et al.* 2009a). TMEM16A-transfected HEK-293 cells were identified by enhanced green fluorescent protein (EGFP) fluorescence using an Olympus IX70 microscope (Olympus, Japan) equipped with the appropriate filter. TMEM16A currents were recorded in the whole-cell configuration in voltage-clamp mode as described for taste bud cells. Cells were kept in mammalian Ringer solution composed of (in mM) 140 NaCl, 5 KCl, 2 CaCl<sub>2</sub>, 1 MgCl<sub>2</sub>, 10 glucose and 10 Hepes, pH 7.4 with NaOH. The pipette solution contained (in mM): 140 NMDG-Cl, 10 HEDTA, 10 Hepes, 1.242 CaCl<sub>2</sub> adjusted to pH 7.3 with NMDG to obtain the final concentration of 0.5  $\mu$ M free Ca<sup>2+</sup>. The extracellular solution contained (in mM): 140 NMDG-Cl, 2 CaCl<sub>2</sub>, 1 MgCl<sub>2</sub>, 10 Hepes, adjusted to pH 7.4 with NMDG. Ani-9 was prepared in DMSO at 10 mM as a stock solution and diluted in the extracellular solution to the final concentration of 1  $\mu$ M.

### Analysis of electrophysiological data

Igor Pro software (WaveMetrics, Lake Oswego, OR, USA) was used for data analysis and to produce the figures. All averaged data from individual experiments in different cells are presented as mean  $\pm$  standard deviation and number of cells (*n*). Statistical analyses of normally distributed data (Shapiro–Wilk test) were performed using unpaired *t* tests. For not normally distributed data, the Mann–Whitney *U*-test was used. The homogeneity of the variance was tested using Levene's test. *P* values of <0.05 were considered statistically significant.

## Results

### RT-PCR

To evaluate the expression of *Tmem16a* and *Tmem16b* transcripts in taste buds, we performed RT-PCR analysis on whole mRNA extract from vallate papillae (Fig. 1). To check the integrity and specificity of the mRNA extracts, we amplified markers for the three types of taste bud cells: *Entpd2* for type I, *Plc $\beta$ 2* for type II and *Snap25* for type III, and for the housekeeping gene *Gapdh* (Fig. 1B). By using primers that span specific and conserved regions from *Tmem16a* and *Tmem16b* sequences, to recognize all isoforms described for both proteins (O'Driscoll *et al.* 2011; Ponissery Saidu *et al.* 2013), we amplified *Tmem16a*, but not *Tmem16b* mRNA (Fig. 1A). As lack of *Tmem16b* transcript amplification could be due to problems in the primers themselves, we validated them by performing RT-PCR on whole mRNA extracts from the olfactory epithelium, where expression of *Tmem16a* and *Tmem16b* is well established (Dauner *et al.* 2012; Maurya & Menini, 2014). RT-PCR from the olfactory epithelium showed the expression of both *Tmem16a* and *Tmem16b* trans-

cripts (Fig. 1C), confirming primer integrity. These results indicate that *Tmem16a*, but not *Tmem16b*, transcripts are expressed in mouse vallate papillae.

### Expression of TMEM16A in taste buds of vallate papillae

To examine the expression and localization of the TMEM16A and TMEM16B proteins in mouse taste buds from vallate papillae, we performed immunohistochemistry and used KO mice as controls (Figs 2 and 3). Figure 2B shows that TMEM16A was expressed in taste buds from adult mice, with a more intense staining near the apical tip. To verify the specificity of the TMEM16A antibody, we performed control experiments using *Tmem16a* KO mice (Fig. 2C and D). As these mice die a few days after birth (Rock *et al.* 2008), we could not test adult animals, but we compared results from WT

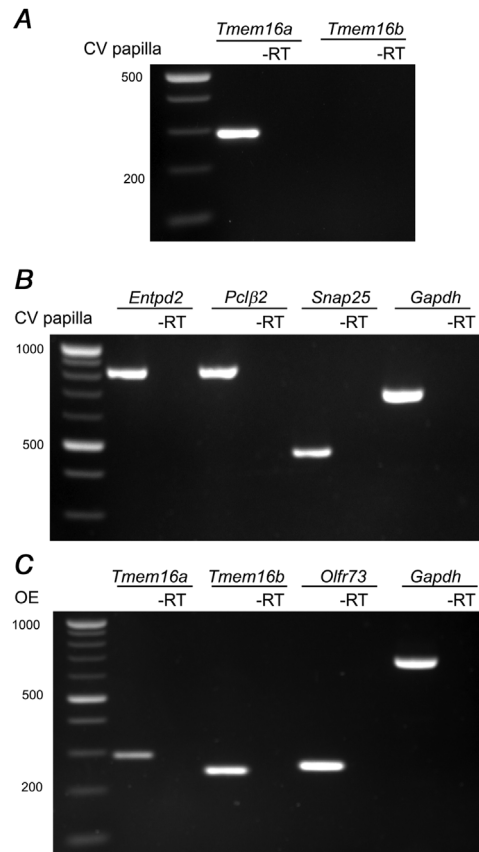


**Figure 1. TMEM16A mRNA is expressed in vallate taste buds**  
Total mRNA extracted from vallate papillae (VP) was amplified by RT-PCR using specific primers for: (A) *Tmem16a* and *Tmem16b*, and (B) *Entpd2*, *Plc $\beta$ 2*, *Snap25* and *Gapdh*. C, to test primer efficiency, total mRNA extracted from the whole olfactory epithelium (OE) was amplified for *Tmem16a*, *Tmem16b*, *Olf73* and *Gapdh*. Control experiments were made using the same sample template without retro-transcriptase.

and KO mice of about the same age (P8–P10). We found no signal for *Tmem16a* in KO mice (Fig. 2D), confirming the specificity of the immunostaining for TMEM16A obtained in WT mice.

By contrast, we did not detect immunoreactivity to TMEM16B in taste buds. Figure 3 shows a comparison between confocal micrographs from sections of mouse vallate papilla (top row) and olfactory epithelium (bottom row). TMEM16B immunoreactivity was absent in taste buds (Fig. 3B), although the same antibody revealed the expression of TMEM16B at the apical surface of the olfactory epithelium (Fig. 3E), as previously shown (Maurya *et al.* 2015; Dibattista *et al.* 2017). We further investigated the expression of TMEM16B in taste buds by taking advantage of a *Tmem16b* KO mice line that was engineered to express mCherry in cells that normally express TMEM16B (Zhang *et al.* 2017). It is important to note that the use of mCherry *Tmem16b* KO mice allows the visualization of the entire cells including all membranes that allow farnesylated mCherry to associate with. As a positive control, we used the olfactory epithelium, where TMEM16B is expressed at the apical side of olfactory sensory neurons (Fig. 3E). Figure 3F shows that mCherry was expressed, as expected, in the entire olfactory neurons of KO mice, including cilia, dendrites, somas and axons. By contrast, mCherry was not

expressed in taste buds (Fig. 3C), further indicating that TMEM16B is not expressed in mouse vallate papillae.

To identify which cell types express TMEM16A in the taste buds, we performed immunohistochemistry using specific markers for each cell type. Indeed, taste buds are composed of three major cell types, characterized by their morphology and expression of specific proteins (Liman *et al.* 2014; Roper & Chaudhari, 2017; Kinnamon & Finger, 2019). Type I cells are often identified by NTPDase2 expression (Bartel *et al.* 2006) and also strongly express at their apical tip the inwardly rectifying potassium channel KCNJ1 (Dvoryanchikov *et al.* 2009). Type II cells specifically express PLC $\beta$ 2 (Zhang *et al.* 2003), while GAD-67 can be used to stain a subset of type III cells (DeFazio *et al.* 2006; Tomchik *et al.* 2007). Figure 4A–C shows that TMEM16A was mainly expressed at the apical part of the taste buds and it was difficult to assess co-expression with NTPDase2, PLC $\beta$ 2 or GAD-67. Lack of co-localization of TMEM16A with these cell markers can be explained because of the different sub-cellular expression. We took advantage of the specific expression of KCNJ1 at the apical tips of type I cells, and we evaluated the co-localization of this marker with TMEM16A. Figure 4D–F shows that TMEM16A co-localized with KCNJ1 at the apical tip of taste buds, indicating the expression of TMEM16A in type I cells.

Together, these results show that TMEM16A, but not TMEM16B, is expressed in taste buds of vallate papillae, and that TMEM16A is mainly localized at the apical part of type I cells.

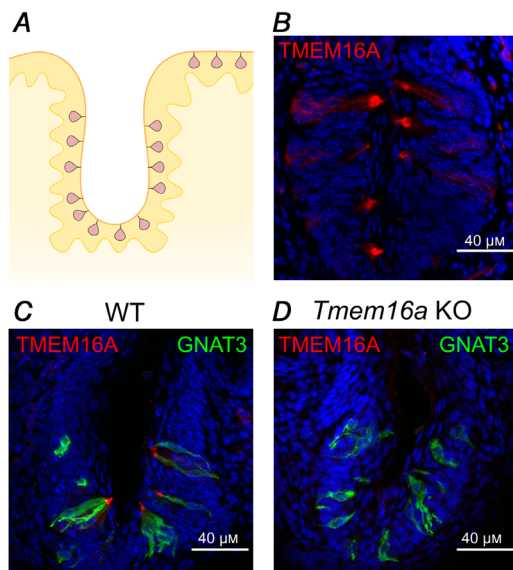


**Figure 2. TMEM16A is expressed in vallate taste buds**

A, schematic drawing of a coronal section of a portion of a vallate papilla (VP) showing the distribution of taste buds. B, confocal micrograph of a coronal section of a vallate papilla immunostained for TMEM16A. TMEM16A was mainly expressed at the apical part of taste buds. C and D, confocal micrographs of sections of vallate papillae from WT (P10) or *Tmem16a* KO (P8) mice immunostained for TMEM16A (red) and GNAT3 (green). No immunoreactivity to TMEM16A was detected from KO tissue. Cell nuclei were stained by DAPI (blue).

### Ca<sup>2+</sup>-activated Cl<sup>-</sup> currents in taste cells

We investigated whether taste cells have functional Ca<sup>2+</sup>-activated Cl<sup>-</sup> channels and compared whole-cell recordings in dissociated cells dialysed with intracellular solutions in the presence or in the absence of 1.5  $\mu$ M free Ca<sup>2+</sup>.

In a first set of experiments, we evaluated the viability of electrophysiological recordings and the possibility to identify the three types of taste cells using a KCl-based intracellular solution in the absence of Ca<sup>2+</sup>. Indeed, it is difficult to identify the dissociated cell types by their morphology, but their electrophysiological fingerprint can be used to identify them. It has been shown that, in physiological solutions, type I cells are characterized by the presence of only voltage-gated outward K<sup>+</sup> currents, type II cells by the combination of voltage-gated inward Na<sup>+</sup> and non-selective outward currents, and type III cells by both voltage-gated inward Na<sup>+</sup> and outward K<sup>+</sup> currents (Bigiani, 2001; Medler *et al.* 2003; Noguchi *et al.* 2003; Romanov & Kolesnikov, 2006; Vandenbeuch *et al.* 2008). Figure 5A shows representative recordings from taste cells displaying three different patterns of currents typical of

the different cell types: (i) cells with only outward currents (type I, green traces); (ii) cells with small inward and large outward currents (type II, blue traces); and (iii) cells with large inward and outward currents (type III, orange traces), indicating that all three cell types are viable in our preparation of dissociated taste cells.

In a second set of experiments, we modified the intracellular solution to suppress outward  $K^+$  currents by replacing  $K^+$  ions with NMDG<sup>+</sup>, a large cation that does not permeate  $K^+$  channels. Figure 5B shows that outward currents were eliminated from type I and type III cells, while large voltage-gated outward currents were still present in type II cells as they are due to the activation of CALHM1/CALHM3 channels, which are characterized by a wide pore with very weak ion selectivity and allow the permeation of large ions, including NMDG<sup>+</sup> (Taruno *et al.* 2013; Ma *et al.* 2016, 2018; Bigiani, 2017). In total, we recorded from 709 viable taste cells and electrophysiologically identified 279 type I (39%), 198 type II (28%) and 232 type III cells (33%).

As our goal was the measurement of  $Ca^{2+}$ -activated  $Cl^-$  currents in electrophysiologically identified cells, we further replaced the external Ringer solution with a one containing only NMDG-Cl and set the resting potential to 0 mV. In these experimental conditions, with NMDG<sup>+</sup>

as the main intra- and extracellular cation, there is no contribution from inward and outward currents due to voltage-gated  $Na^+$  and  $K^+$  channels (Fig. 5C). To investigate the presence of  $Ca^{2+}$ -activated currents in the three types of taste cells, we compared recordings obtained in symmetrical NMDG-Cl solutions with nominally 0  $Ca^{2+}$  or 1.5  $\mu M$  free intracellular  $Ca^{2+}$ . The cell type was determined in external Ringer solution by using the voltage protocol shown at the top of Fig. 5B and then Ringer solution was replaced by NMDG-Cl as in Fig. 5C.

Type II cells showed voltage-gated outward currents slowly activated by depolarization both in the absence and in the presence of 1.5  $\mu M$  intracellular free  $Ca^{2+}$  (Fig. 6A). Average current amplitudes at +100 mV were not significantly different (Fig. 6B;  $P = 0.14$  unpaired  $t$  test), indicating that no additional currents were activated by  $Ca^{2+}$  in type II cells. To further investigate the presence of  $Ca^{2+}$ -activated currents that could be masked by the very large CALHM-mediated outward currents, we blocked these currents by adding 200  $\mu M$   $Gd^{3+}$ , a non-specific ion channel blocker, and verified that also after the blockage the residual outward current amplitudes were not significantly different with 0 or 1.5  $\mu M$   $Ca^{2+}$  (Fig. 6A and B;  $P = 0.57$  Mann-Whitney  $U$ -test). As

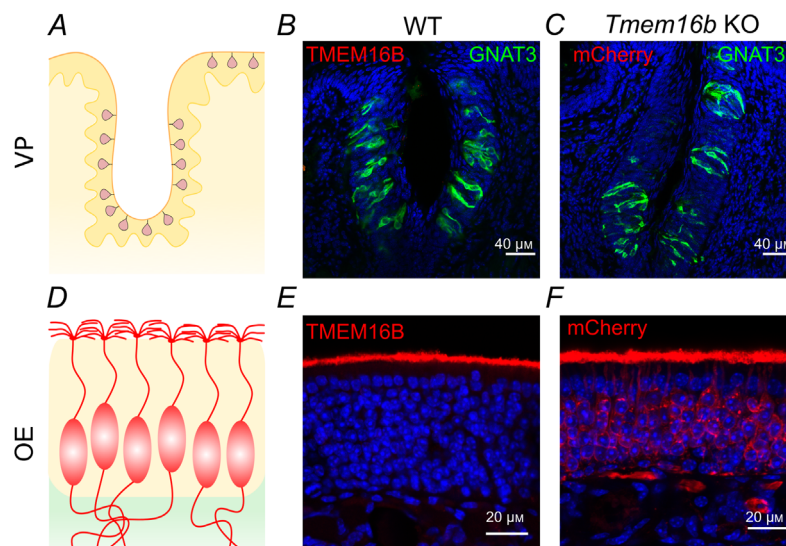


**Figure 3. TMEM16B is not expressed in vallate taste buds**

A, schematic drawing of a coronal section of a vallate papilla (VP) showing the distribution of taste buds. B, confocal micrographs of a vallate papilla from a WT mouse immunostained with antibody against TMEM16B (red) and GNAT3 (green). No immunoreactivity to TMEM16B was detected in taste buds. C, confocal micrograph of a section of a vallate papilla from *Tmem16b* KO mouse expressing mCherry on the membrane of cells that normally express TMEM16B (see Methods for details on the generation of the KO mice by Zhang *et al.* 2017), immunostained with antibody against red fluorescent proteins (red) and GNAT3 (green). No immunoreactivity to mCherry was detected in taste buds from KO, indicating that TMEM16B was not expressed in WT taste buds. D, schematic drawing of a coronal section of the olfactory epithelium (OE) showing olfactory sensory neurons with cilia in the apical layer. E, TMEM16B was normally detected in the apical layer of the WT olfactory epithelium using the same TMEM16B antibody used in B. F, mCherry (red) was detected in olfactory sensory neurons from *Tmem16b* KO mice. In these KO mice, mCherry was expressed, as expected, in the membrane of entire olfactory neurons that normally express TMEM16B at the apical side. Cell nuclei were stained by DAPI (blue).



a control, we also tested if  $Gd^{3+}$  blocks TMEM16A or TMEM16B channels, by recording  $Ca^{2+}$ -activated  $Cl^-$  currents in HEK293T cells transfected with TMEM16A or TMEM16B and did not measure any blocking effect by  $200 \mu M$   $GdCl_3$  on these channels (data not shown).

Type III cells showed negligible currents both in the absence and in the presence of  $1.5 \mu M$   $Ca^{2+}$ , indicating the absence of functional  $Ca^{2+}$ -activated currents in symmetrical NMDG-Cl solutions (Fig. 6C and D;  $P = 0.33$  unpaired  $t$  test).

In type I cells,  $1.5 \mu M$  free  $Ca^{2+}$  generated large currents while currents in  $0$   $Ca^{2+}$  were very small (Fig. 7A and B).  $Ca^{2+}$ -activated currents had the typical time-dependent features of  $Ca^{2+}$ -activated  $Cl^-$  channels, displaying time-dependent deactivation kinetics with hyperpolarizing potentials, activation kinetics with depolarizing potentials, and deactivating inward tail currents when the voltage was stepped to  $-100$  mV at the end of the protocol (Fig. 7A, D and G). The  $I-V$  relationship of the steady-state  $Ca^{2+}$ -activated current at the end of the voltage steps was outwardly rectifying with an average ratio between currents at  $+100$  mV and  $-100$  mV of  $1.6 \pm 0.7$  ( $n = 17$ ).

To examine whether the  $Ca^{2+}$ -activated current in type I cells was carried by  $Cl^-$ , we replaced extracellular  $Cl^-$  with  $MeS^-$ , a large impermeant anion and found that the reversal potential shifted toward a positive value ( $+36 \pm 8$  mV,  $n = 7$ ), as expected for  $Cl^-$  channels, indicating that the  $Ca^{2+}$ -activated current in type I cells is mainly carried by  $Cl^-$  (Fig. 7D–F). We also tested the blockage of  $Ca^{2+}$ -activated  $Cl^-$  currents by Ani-9, a compound that fully blocks TMEM16A in the sub-micromolar range and has a high selectivity for

TMEM16A compared with TMEM16B (Seo *et al.* 2016). Figure 7G and H show that  $1 \mu M$  Ani-9 caused a strong reversible inhibition of the current in WT type I cells, with an average current block of  $75\% \pm 8\%$  at  $+100$  mV and  $90 \pm 5\%$  at  $-100$  mV (Fig. 7I), indicating that the current was mainly carried through TMEM16A channels.

We also performed experiments in type I taste cells from *Tmem16b* KO mice. In agreement with our previous results showing the absence of TMEM16B in taste buds (Figs 1 and 3), we did not find any statistical difference between  $Ca^{2+}$ -activated currents in type I taste cells from WT and *Tmem16b* KO (Fig. 7C). Moreover, the shift of the reversal potential upon replacement of  $Cl^-$  with  $MeS^-$  and the blocking effect of Ani-9 were similar in type I taste cells from WT and *Tmem16b* KO (Fig. 7F and I), in agreement with the previous experiments indicating that TMEM16A is the channel responsible for the measured  $Ca^{2+}$ -activated  $Cl^-$  currents.

To further investigate the possibility that a small inward current could be activated by  $Ca^{2+}$  in type II or III taste cells, we compared recordings in symmetrical NMDG-Cl solutions from the three cell types obtained by holding the cell at  $-100$  mV for several seconds in the presence of  $1.5 \mu M$   $Ca^{2+}$  in the pipette. Figure 8 further shows that large currents blocked by  $1 \mu M$  Ani-9 were activated only in type I cells, while type II and III cells had low-amplitude currents that were not blocked by Ani-9 (Fig. 8A, C and E). Average current amplitudes at  $-100$  mV were  $-1083 \pm 824$  pA ( $n = 17$ ) for type I,  $-68 \pm 95$  pA ( $n = 18$ ) for type II and  $-6 \pm 8$  pA ( $n = 13$ ) for type III cells. Cell viability was tested after application of the blocker (Fig. 8B, D and F). A significant blockage by Ani-9 in type I was observed within a few seconds from the application of the

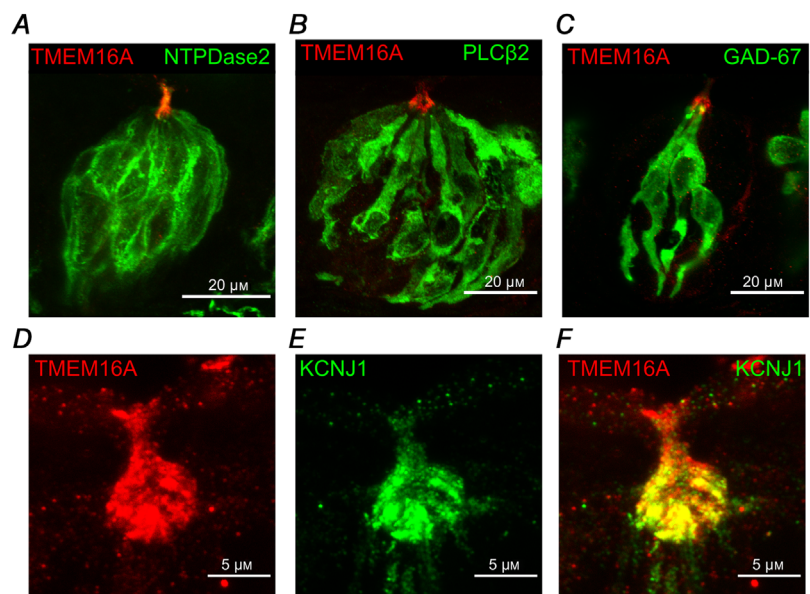


**Figure 4. TMEM16A colocalizes with KCNJ1 in type I taste bud cells**

Confocal micrographs of coronal sections of vallate papillae. A–C, immunostaining for TMEM16A and NTPDase2, PLC $\beta$ 2, and GFP (GAD67-GFP mouse). D–F, immunostaining for TMEM16A (red) and KCNJ1 (green). Merging of the signals shows co-localization of TMEM16A and KCNJ1 at the apical part of taste buds.

blocker and was very similar to that measured in HEK-293 cells transiently transfected with *Tmem16a* (Fig. 9B).

We could not perform experiments in taste cells from *Tmem16A* KO mice because more than 50% of these mice die within 5 days of birth (Rock *et al.* 2008) and, as shown by Bigiani *et al.* (2002), it is difficult to identify taste buds in very young mice, preventing the possibility of obtaining a number of dissociated cells sufficient for electrophysiological experiments.

Collectively, these data show that intracellular  $\text{Ca}^{2+}$  can activate a large  $\text{Cl}^-$  current in type I (but not in type II or III) taste cells, carried through the TMEM16A channel.

### ATP evokes a $\text{Cl}^-$ current in type I taste cells

Studies by Kim *et al.* (2000) and Cherkashin *et al.* (2016) showed that a subpopulation of taste cells exhibited large  $\text{Ca}^{2+}$ -activated  $\text{Cl}^-$  currents when stimulated with

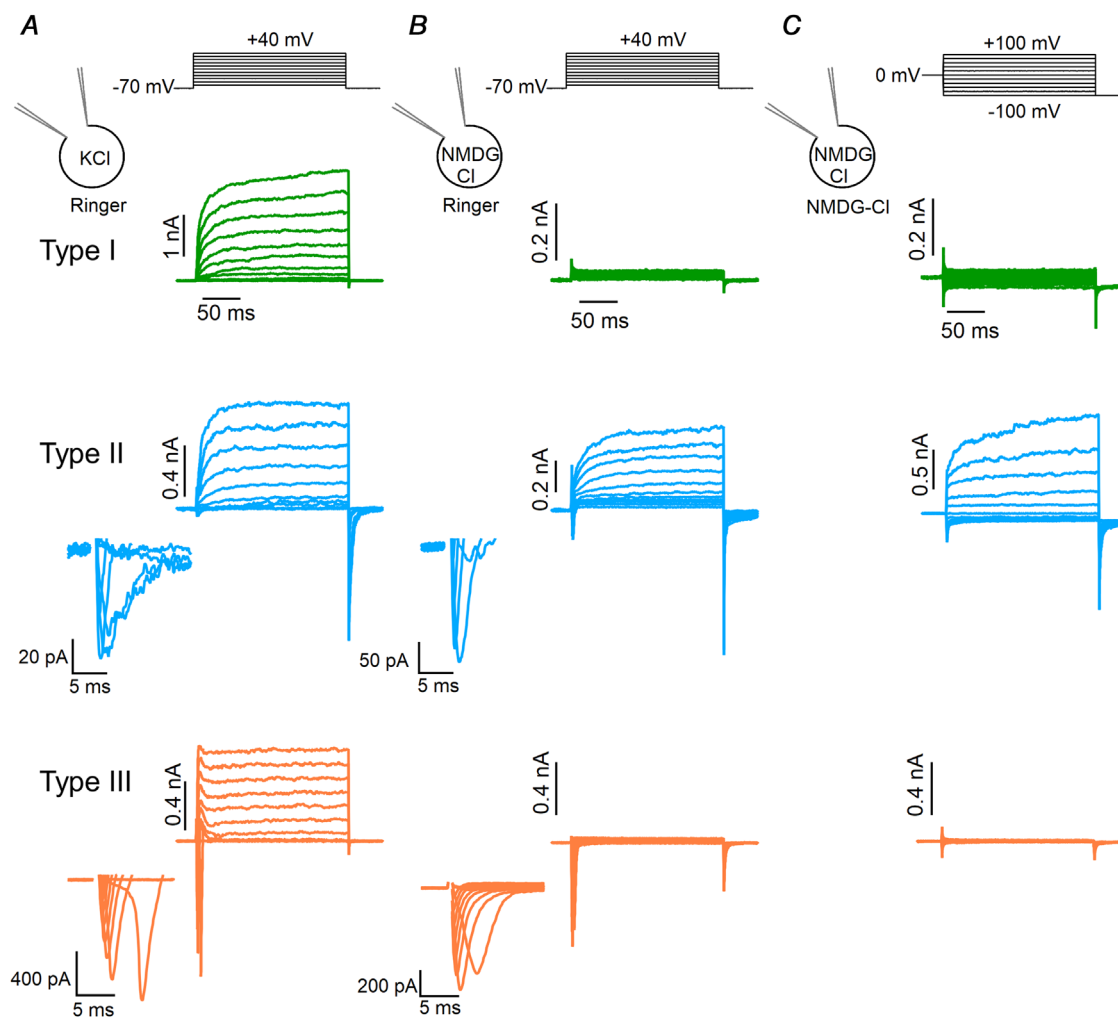


**Figure 5. Electrophysiological identification of taste bud cell types**

A, representative whole-cell recordings obtained with a pipette solution containing KCl from type I (green), II (blue) or III (orange) taste bud cells bathed in mammalian Ringer solution. The holding potential was  $-70$  mV and voltage steps from  $-60$  mV to  $+40$  mV with  $10$  mV increments were applied as shown at the top of the panel. Enlarged transient inward currents of type II and III cells are shown in the insets. B, representative whole-cell recordings using NMDG-Cl in the patch pipette and mammalian Ringer solution as the extracellular solution. The voltage protocol was the same of the recordings shown in A. Voltage-gated outward currents in type I and III cells were abolished by the replacement of  $\text{K}^+$  with  $\text{NMDG}^+$ , whereas they were still recorded in type II cells. C, the same cells in B were bathed in NMDG-Cl symmetrical solutions. Note that the voltage protocol was different from that used in B, as the holding potential was  $0$  mV and voltage steps from  $-100$  mV to  $+100$  mV with  $20$  mV increments were applied followed by a step to  $-100$  mV, as indicated at the top of the panel. In these conditions, type I and III cells did not show voltage-gated inward and outward currents, whereas type II cells still had robust voltage-gated outward currents. Intracellular solutions always contained nominally  $0$   $\text{Ca}^{2+}$ .

P2Y receptor agonists. Perforated patch recordings showed that the subpopulation consisted of type I cells (Cherkashin *et al.* 2016). Here, we used whole-cell recordings instead of perforated patch to test whether ATP stimulation could activate  $\text{Ca}^{2+}$ -activated  $\text{Cl}^-$  currents in type I cells. We found that  $50 \mu\text{M}$  ATP at the holding potential of  $-70 \text{ mV}$  induced large inward currents in 71% of type I taste cells (89 out of 125) in extracellular Ringer solution (Fig. 10A). ATP-evoked currents were still present when NaCl in the Ringer solution was replaced with NMDG-Cl and  $0 \text{ K}^+$ , indicating that the inward current was not carried by  $\text{Na}^+$  or  $\text{K}^+$  (Fig. 10B).

To measure the  $I$ - $V$  relationship and to determine the ionic selectivity of the ATP-induced current, we applied voltage ramps before and during ATP stimulation in various ionic conditions (Fig. 10C and D). The  $I$ - $V$  relationship of the current activated by ATP was calculated by subtracting the current generated by the voltage ramp before stimulation (Fig. 10E and F). Rectification properties in Ringer varied in different cells from outward to linear rectification, with an average ratio of the current amplitude at  $+60 \text{ mV}$  and  $-60 \text{ mV}$  of  $1.3 \pm 0.6$  ( $n = 18$ , Fig. 10G). Different rectifications are probably due to different intracellular  $\text{Ca}^{2+}$  concentrations elicited by ATP. The average reversal potential was  $-6 \pm 8 \text{ mV}$  ( $n = 20$ ) in Ringer solution and shifted to  $+40 \pm 9 \text{ mV}$  ( $n = 7$ ) upon reduction of the extracellular  $\text{Cl}^-$  concentration by

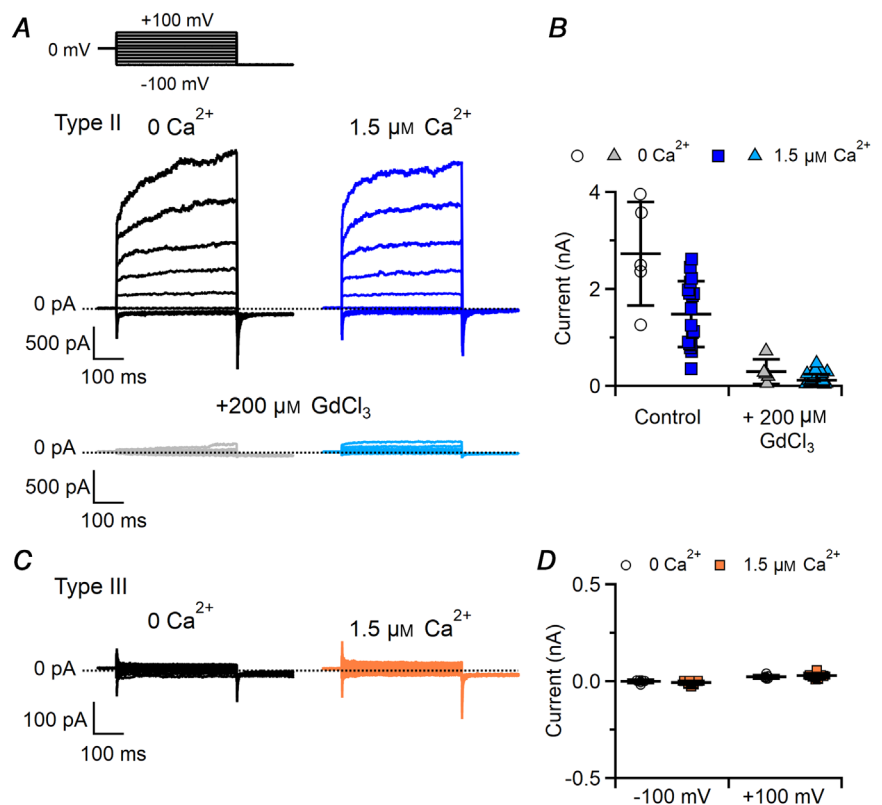
replacing NaCl with sodium gluconate, indicating that the current was mainly carried by  $\text{Cl}^-$  (Fig. 10H). To test whether the ATP-induced  $\text{Cl}^-$  current was due to activation of TMEM16A, we applied the specific blocker Ani-9. Figure 10H shows that Ani-9 caused a sudden reduction of the inward current with a time course similar to that observed in HEK-293 transiently transfected with TMEM16A (Fig. 9B), indicating that the  $\text{Cl}^-$  current was carried through TMEM16A channels. However, we cannot completely exclude the possibility that a prolonged application of Ani-9 could have a non-specific action and perhaps inhibit ATP-induced  $\text{Ca}^{2+}$  signals as observed in some cell lines (Centeio *et al.* 2020).

Thus, our results in the whole-cell configuration confirm previous data obtained with perforated patch recordings (Kim *et al.* 2000; Cherkashin *et al.* 2016) showing that ATP evokes large  $\text{Ca}^{2+}$ -activated  $\text{Cl}^-$  currents in type I cells and extend those results showing that these currents are blocked by Ani-9, consistent with our data indicating that these currents are due to activation of TMEM16A channels.

## Discussion

In this study, we have demonstrated that a large  $\text{Ca}^{2+}$ -activated  $\text{Cl}^-$  current can be physiologically activated in type I taste bud cells, but not in type II

**Figure 6. Type II and III taste bud cells do not have  $\text{Ca}^{2+}$ -activated  $\text{Cl}^-$  currents**  
Representative whole-cell recordings from type II (A) and type III (C) taste cells obtained in symmetrical NMDG-Cl solutions. The pipette solution contained nominally  $0 \text{ Ca}^{2+}$  or  $1.5 \mu\text{M} \text{ Ca}^{2+}$  as indicated. The holding potential was  $0 \text{ mV}$  and voltage steps from  $-100 \text{ mV}$  to  $+100 \text{ mV}$  with  $20 \text{ mV}$  increments were applied followed by a step to  $-100 \text{ mV}$ , as indicated at the top of A.  $\text{Gd}^{3+}$  at  $200 \mu\text{M}$  was added to block the large CALHM-mediated outward currents in type II cells. B and D, scatter dot plots with averages  $\pm$  SD showing current amplitudes in  $0$  or  $1.5 \mu\text{M} \text{ Ca}^{2+}$  in type II (B), currents at  $+100 \text{ mV}$  in the absence or in the presence of  $200 \mu\text{M} \text{ Gd}^{3+}$ ,  $n = 5$ – $18$ ;  $P = 0.14$  unpaired  $t$  test for control;  $P = 0.57$  Mann-Whitney  $U$ -test for  $\text{Gd}^{3+}$ ) or type III taste cells (D,  $n = 6$ – $13$ ;  $P = 0.26$  unpaired  $t$  test for  $-100 \text{ mV}$ ;  $P = 0.33$  unpaired  $t$  test for  $+100 \text{ mV}$ ).



and III taste bud cells. Moreover, we have shown that the  $\text{Ca}^{2+}$ -activated  $\text{Cl}^-$  channel TMEM16A, but not TMEM16B, is expressed mainly at the apical part of type I cells where it largely colocalizes with the inwardly rectifying  $\text{K}^+$  channel KCNJ1.

### $\text{Ca}^{2+}$ -activated $\text{Cl}^-$ channels in taste bud cells

Our study confirms some data of the previous pioneering reports showing the presence of  $\text{Ca}^{2+}$ -activated  $\text{Cl}^-$

currents in taste cells and significantly extends and revises them (Cherkashin *et al.* 2016; Kim *et al.* 2000). Indeed, Kim *et al.* (2000) used perforated patch-clamp recordings combined with  $\text{Ca}^{2+}$  imaging and demonstrated that intracellular  $\text{Ca}^{2+}$  increase, produced by ionomycin or by ATP, activated  $\text{Cl}^-$  currents in a subpopulation of taste cells, which exhibited no voltage-gated  $\text{Na}^+$  and  $\text{Ca}^{2+}$  currents. The same authors also showed that the cytosolic  $\text{Ca}^{2+}$  increase produced by ATP was mediated by P2Y receptors, demonstrating that ATP indirectly activated  $\text{Cl}^-$  channels by causing  $\text{Ca}^{2+}$  release from intracellular

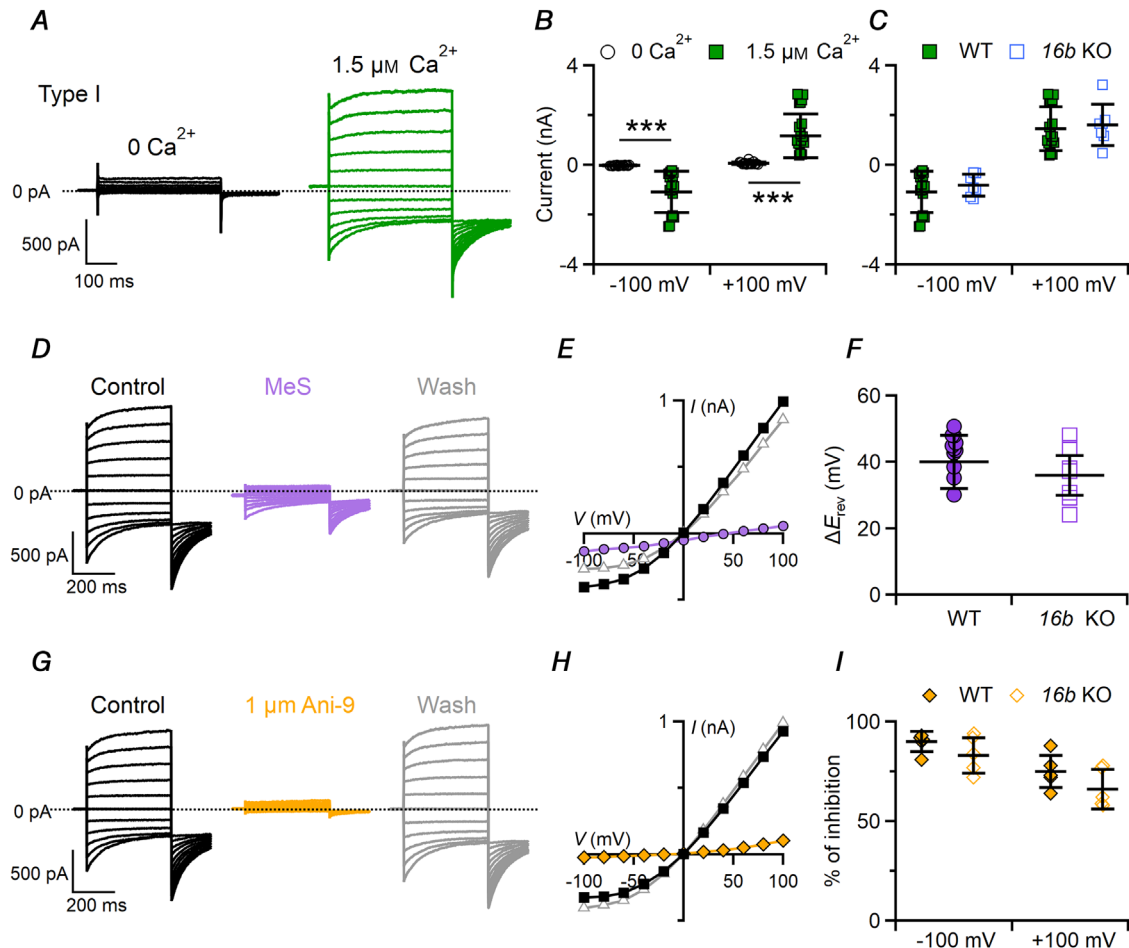


**Figure 7.  $\text{Ca}^{2+}$ -activated  $\text{Cl}^-$  currents in type I taste bud cells**

A, representative whole-cell recordings from type I taste cells measured in symmetrical NMDG-Cl solutions with an intracellular solution containing nominally 0  $\text{Ca}^{2+}$  or 1.5  $\mu\text{M}$   $\text{Ca}^{2+}$ . The holding potential was 0 mV, and voltage steps from -100 mV to +100 mV with 20 mV increments were applied followed by a step to -100 mV. B and C, scatter dot plots with averages  $\pm$  SD showing (B) current amplitudes measured at steady state in 0 or 1.5  $\mu\text{M}$   $\text{Ca}^{2+}$  ( $n = 15-17$ ,  $***P = 3.5 \times 10^{-9}$ , -100 mV,  $P = 3.4 \times 10^{-9}$ , +100 mV, Mann-Whitney U-test) and (C)  $\text{Ca}^{2+}$ -activated currents in cells from WT ( $n = 15$ ) or *Tmem16B* KO ( $n = 7$ ;  $P = 0.8$ , -100 mV,  $P = 0.41$ , +100 mV, Mann-Whitney U-test) mice. D and G, the same cell was exposed to a control solution containing NMDG-Cl (black traces), or NMDG-MeS (purple traces) or NMDG-Cl with 1  $\mu\text{M}$  Ani-9 (yellow traces), followed by washout in NMDG-Cl (grey traces). E and H, steady-state  $I-V$  relationships measured at steady state from the recordings shown in D and G in control condition (squares), MeS (E, circles) or 1  $\mu\text{M}$  Ani-9 (H, diamonds) and after washout (triangles). F and I, scatter dot plots with average  $\pm$  SD showing (F)  $\Delta E_{\text{rev}}$  (mV) after MeS perfusion in cells from WT ( $n = 11$ ) and *Tmem16b* KO ( $n = 7$ ;  $P = 0.08$  unpaired  $t$  test) mice, and (I) percentage of current inhibition by 1  $\mu\text{M}$  Ani-9 measured at -100 and +100 mV in cells from WT ( $n = 5$ ) and *Tmem16b* KO mice ( $n = 5$ ;  $P = 0.27$  unpaired  $t$  test for -100 mV;  $P = 0.2$  unpaired  $t$  test for +100 mV) mice.

stores. Cherkashin *et al.* (2016) further investigated the distribution of  $\text{Ca}^{2+}$ -activated  $\text{Cl}^-$  currents in taste cell types using the perforated patch clamp technique. They found clear evidence that type I cells have functional  $\text{Ca}^{2+}$ -activated  $\text{Cl}^-$  channels that can be activated by ionomycin or purinergic agonists. By measuring the effect of available blockers for TMEM16A, they found that channels in type I cells were blocked by CaCCinh-A01 but not by T16Ainh-A01. The authors also recorded a very small inward current in type II cells activated by ionomycin or by photorelease of caged  $\text{Ca}^{2+}$  that could be blocked by T16Ainh-A01. Type III cells exhibited no ion current induced by ionomycin or photorelease of caged Ca. In addition, the same authors found transcripts of *Tmem16a* and *Tmem16b* in vallate papillae and confirmed their expression by using immunohistochemistry. They also identified *Tmem16a* transcripts in type II cells, and *Tmem16b* transcripts in both type I and type II cells. On the basis of their results, Cherkashin *et al.* (2016) concluded that type I cells express only TMEM16B, while type II cells express both TMEM16A and TMEM16B channels.

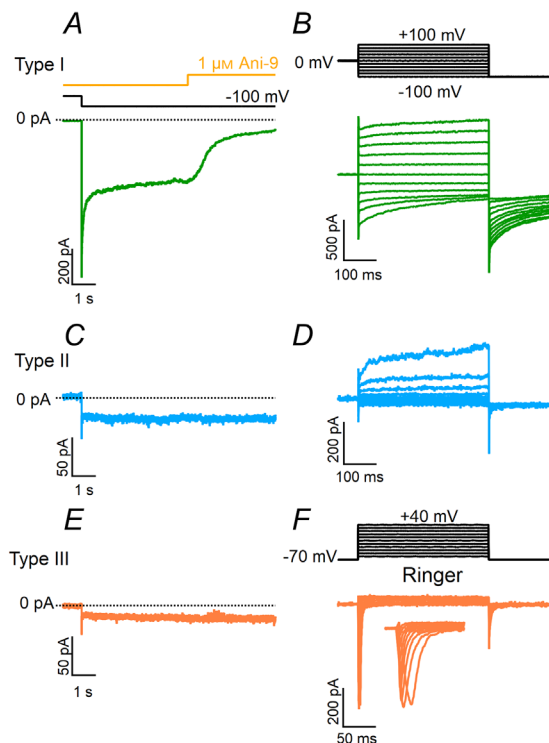


**Figure 8. Blockage of inward currents by Ani-9**

A, C and E, representative whole-cell recordings from type I (green traces), II (blue traces) or III (orange traces) taste cells recorded in symmetrical NMDG-Cl solutions with an intracellular solution containing  $1.5 \mu\text{M}$   $\text{Ca}^{2+}$ . The holding potential was 0 mV and was stepped to  $-100$  mV as indicated. Ani-9 at  $1 \mu\text{M}$  was applied as indicated in the upper trace. B, D and F, after the application of Ani-9, cell viability was tested with the indicated voltage protocols. The extracellular solution was NMDG-Cl in B and D or Ringer in F.

In our study, we used a more recently discovered selective blocker of TMEM16A, Ani-9 (Seo *et al.* 2016), and we were able to use KO mice for *Tmem16a* and *Tmem16b* as a control for the specificity of antibodies. This allowed us to confirm, revise and extend some of the previous discoveries. By using specific antibodies for TMEM16A and TMEM16B validated on tissues from KO mice, we confirmed the expression of TMEM16A in taste buds whereas we did not find expression of TMEM16B. We further investigated the expression of TMEM16B by using the *Tmem16b* KO mice line engineered by Zhang *et al.* (2017) to express mCherry under the *Tmem16b* promoter. We confirmed that mCherry was not expressed in taste buds, whereas it was expressed by olfactory sensory neurons in the olfactory epithelium, further showing that TMEM16B is not expressed in taste buds.

From a functional point of view, we performed patch-clamp experiments in the whole-cell configuration and compared recordings obtained with nominally 0 or  $1.5 \mu\text{M}$  intracellular  $\text{Ca}^{2+}$  and measured large  $\text{Ca}^{2+}$ -activated  $\text{Cl}^-$  current in type I cells blocked by Ani-9, a selective blocker of TMEM16A, whereas we could not measure any  $\text{Ca}^{2+}$ -activated  $\text{Cl}^-$  current in type II and type III cells. Moreover, in type I cells, extracellular

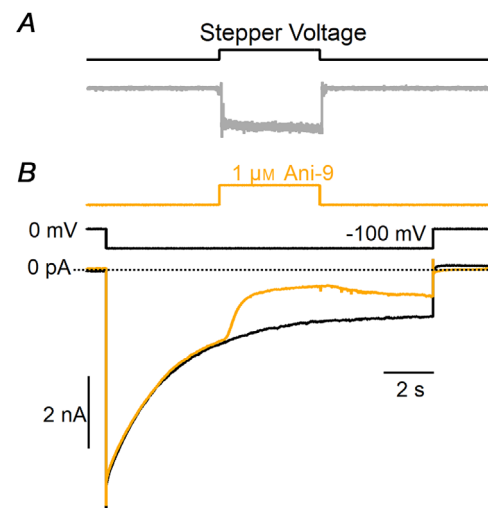


**Figure 9. Blockage of TMEM16A-mediated current in HEK-293 cells by Ani-9**

A, the upper trace shows the voltage command of the stepper motor moving glass pipes in which different solutions were flowing. The bottom trace shows the time course of the solution exchange from Ringer solution to 1 M KCl moving the pipes in front of a patch electrode. The change of solution was obtained in less than 50 ms. B, representative whole-cell recordings from HEK-293 cells expressing TMEM16A recorded in symmetrical NMDG-Cl solutions with an intracellular solution containing  $0.5 \mu\text{M}$   $\text{Ca}^{2+}$ . The holding potential was 0 mV and was stepped to  $-100$  mV as indicated. Ani-9 at  $1 \mu\text{M}$  was applied as indicated in the upper trace. A significant reduction of the currents was observed within a few seconds from the application of the blocker.

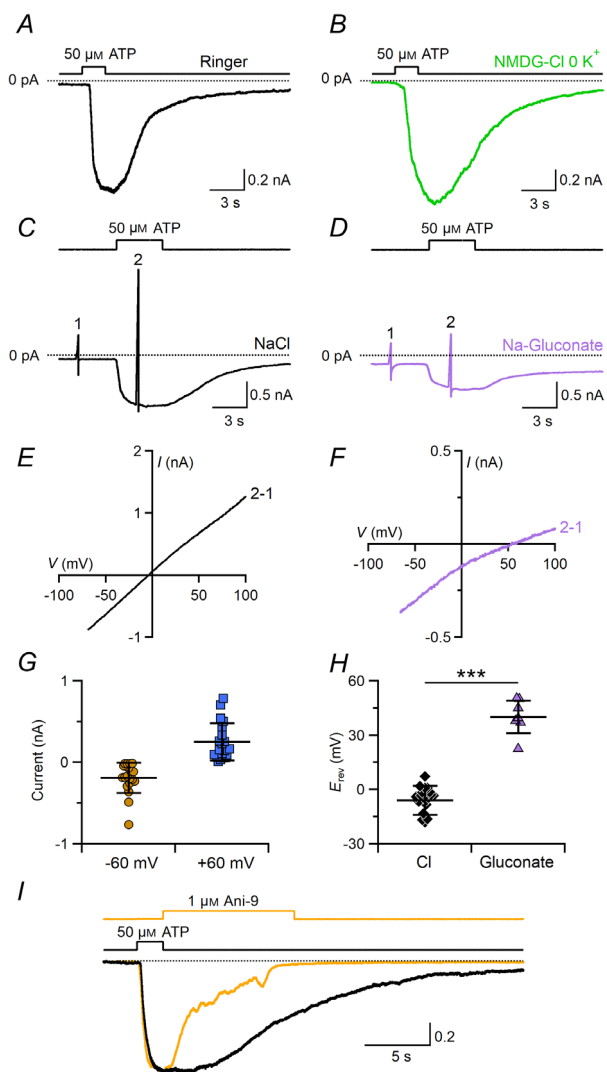


**Figure 10. ATP induces a  $\text{Cl}^-$  current blocked by Ani-9 in type I taste bud cells**

Representative whole-cell recordings from type I taste cells stimulated with  $50 \mu\text{M}$  ATP in Ringer solution (A) or in a Ringer solution modified by replacing NaCl with NMDG-Cl and omitting  $\text{KCl}$  (B). The pipette solution contained NMDG-Cl. The holding potential was  $-70$  mV. ATP was applied for the time indicated in the upper trace. C and D, voltage ramps from  $-70$  to  $+100$  mV before (1) and during (2) ATP application were used to measure  $I$ - $V$  relationships in the presence of Ringer solution with NaCl or Ringer solution with sodium gluconate (D). E and F,  $I$ - $V$  relationships from the cells shown in C and D respectively obtained by subtracting the traces (1) from those in the presence of ATP (2). G, scatter dot plots with averages  $\pm$  SD of current amplitudes at  $-60$  and  $+60$  mV ( $n = 18$ ). H, scatter dot plots with averages  $\pm$  SD of  $E_{\text{rev}}$  recorded in Ringer solution with NaCl ( $n = 20$ , black diamonds) or in Ringer solution with sodium gluconate ( $n = 7$ , purple triangles;  $P = 1.93 \times 10^{-11}$  unpaired  $t$  test). I, blockage by  $1 \mu\text{M}$  Ani-9 of the ATP-induced current in Ringer solution. ATP and Ani-9 were applied as indicated in the upper traces. Currents from the same cell were normalized to the peak amplitude. ATP stimulus duration was 2 s. Ani-9 was applied after ATP for 10 s and completely blocked the current (yellow trace,  $-756$  pA peak current). Control trace recorded after Ani-9 application (black trace,  $-948$  pA peak current).

ATP produced activation of a large  $\text{Cl}^-$  current that was inhibited by Ani-9, further demonstrating the functional expression of TMEM16A in type I cells.

Recently, Ávalos Padro *et al.* (2021) reported that the interaction of TMEM16A with KCNE1 switches the gating mode of TMEM16A from  $\text{Ca}^{2+}$ -dependent to voltage-dependent, showing that TMEM16A could also be activated in the absence of  $\text{Ca}^{2+}$  if it is associated with KCNE1. However, our data show that type II and type III cells lack voltage-gated  $\text{Cl}^-$  currents also in nominally 0 intracellular  $\text{Ca}^{2+}$  (Fig. 6), further excluding the possibility that TMEM16A could be active in these cell types.

As type II cells are very heterogeneous (Chandrashekar *et al.* 2006), we cannot exclude the possibility that some rare type II cells could exhibit  $\text{Ca}^{2+}$ -activated  $\text{Cl}^-$  currents.

### Physiological activators and role of $\text{Ca}^{2+}$ -activated $\text{Cl}^-$ currents in type I taste bud cells

Type I cells comprise about 50% of the cells in each taste bud and are considered to have mainly glial-like functions. Not much is known about their physiological roles, which still need to be extensively investigated. It is well established that ATP is released from type II taste cells and is degraded by NTPDase2 on the surface of type I cells (Bartel *et al.* 2006; Vandenbeuch *et al.* 2013). However, type I cells also express P2Y receptors that have been shown to increase cytosolic  $\text{Ca}^{2+}$  when activated by ATP (Bystrova *et al.* 2006; Kim *et al.* 2000). Immunohistochemical data showed that P2Y<sub>1</sub> receptors (Kataoka *et al.* 2004) and P2Y<sub>2</sub> receptors (Bystrova *et al.* 2006) are expressed in the basolateral membrane of a subset of taste bud cells. Thus, we speculate that ATP released through CALHM1/CALHM3 channels of type II cells reaching the surface of type I cells, where it is degraded by NTPDase2, can also bind to P2Y receptors, and indirectly activate TMEM16A channels causing a flux of  $\text{Cl}^-$  according to its electrochemical gradient.

In addition to P2Y receptors, type I cells also express other receptors that, upon activation by their agonists, produce an increase in intracellular  $\text{Ca}^{2+}$  and can therefore activate TMEM16A channels. Sinclair *et al.* (2010) have shown that a subset of type I cells express the oxytocin receptor that upon stimulation by oxytocin causes an intracellular  $\text{Ca}^{2+}$  increase similar to that induced by ATP. In another study, Huang & Wu (2018) measured  $\text{Ca}^{2+}$  release from intracellular stores in type I cells in response to substance P.

What, then, is the physiological role of  $\text{Ca}^{2+}$ -activated  $\text{Cl}^-$  channels in type I taste cells? Depending on the  $\text{Cl}^-$  equilibrium potential and on the membrane potential, these channels may allow influx or efflux of  $\text{Cl}^-$ , increasing or decreasing the cytoplasmic  $\text{Cl}^-$  concentration and

contributing to cell hyperpolarization or depolarization. At present, estimates of the  $\text{Cl}^-$  concentration inside taste cells are not available and may differ between the basolateral and apical sides. The extracellular  $\text{Cl}^-$  concentration varies depending on apical or basolateral parts of the cell. Indeed, the apical part of taste cells is likely to be immersed in saliva, while the cell body is surrounded by interstitial fluid. Saliva has a naturally low  $\text{Cl}^-$  concentration, being composed of 15 mM NaCl, 22 mM KCl, 3 mM  $\text{CaCl}_2$  and 0.6 mM  $\text{MgCl}_2$ , corresponding to a  $\text{Cl}^-$  concentration of about 44 mM (Breza *et al.* 2010; Matsuo, 2000), while the interstitial fluid contains about 100–110 mM  $\text{Cl}^-$  (Yunos *et al.* 2010). However, when salty tastants enter the taste pore, the concentration of  $\text{Cl}^-$  can greatly increase, modifying the  $\text{Cl}^-$  equilibrium potential.

We have shown that TMEM16A largely colocalized with the inwardly rectifying  $\text{K}^+$  channel KCNJ1 at the apical part of type I cells. KCNJ1 has been proposed to be involved in buffering of basolateral extracellular  $\text{K}^+$  by mediating the  $\text{K}^+$  efflux through the apical pore (Dvoryanchikov *et al.* 2009). As stimulation by tastants of type II cells produces both the local increase of extracellular  $\text{K}^+$  and release of ATP, we speculate that the activation of TMEM16A by ATP could mediate an influx of  $\text{Cl}^-$  allowing a sustained apical extrusion of  $\text{K}^+$ .

Interestingly, it has been shown that TMEM16A can be activated in the absence of intracellular  $\text{Ca}^{2+}$  by low extracellular pH through the titration of glutamic acid 623 (Cruz-Rangel *et al.* 2017). We speculate that this modulation could be relevant during sour stimulation of type III cells. Indeed, the activation of TMEM16A by low pH could contribute, together with KCNJ1, to buffer the increase of extracellular  $\text{K}^+$  due to action potential firing of type III cells. However, Cruz-Rangel *et al.* (2017) also showed that an increase in intracellular  $\text{Ca}^{2+}$  to about 1  $\mu\text{M}$  abolished the pH-dependent gating of TMEM16A. Moreover, because TMEM16A has different permeabilities for anions, it is tempting to speculate that this channel may contribute to the long known 'anion effect' in which responses to sodium salts differ depending on the anion (Beidler, 1953; Breza & Contreras, 2012; Roebber *et al.* 2019).

Finally, it is of interest to note that Tizzano *et al.* (2015) have shown that human vallate papillae share most of the structural, morphological and molecular features observed in rodents, and therefore future work should also investigate the expression of TMEM16A and verify a possible physiological role of this channel in human taste buds.

In summary, our data provide a definitive demonstration that TMEM16A-mediated currents are functional in type I taste cells of mouse vallate papillae and provide a foundation for future studies investigating additional physiological roles for type I cells, often

neglected with respect to studies on the type II and III taste cells.

## References

- Ávalos Padro P, Häfner S, Comoglio Y, Wdziekonski B, Durantón C, Attali B, Barhanin J & Sandoz G (2021). KCNE1 is an auxiliary subunit of two distinct ion channel superfamilies. *Cell* **184**, 534–544.e11.
- Barry PH (1994). JPCalc, a software package for calculating liquid junction potential corrections in patch-clamp, intracellular, epithelial and bilayer measurements and for correcting junction potential measurements. *J Neurosci Methods* **51**, 107–116.
- Bartel DL, Sullivan SL, Lavoie EG, Sévigny J & Finger TE (2006). Nucleoside triphosphate diphosphohydrolase-2 is the ecto-ATPase of type I cells in taste buds. *J Comp Neurol* **497**, 1–12.
- Baumer-Harrison C, Raymond MA, Myers TA, Sussman KM, Rynberg ST, Ugartechea AP, Lauterbach D, Mast TG & Breza JM (2020). Optogenetic stimulation of type I GAD65+ cells in taste buds activates gustatory neurons and drives appetitive licking behavior in sodium-depleted mice. *J Neurosci* **40**, 7795–7810.
- Bébé P, DeSimone JA, Avenet P & Lindemann B (1990). Membrane currents in taste cells of the rat fungiform papilla. Evidence for two types of Ca currents and inhibition of K currents by saccharin. *J Gen Physiol* **96**, 1061–1084.
- Beidler LM (1953). Properties of chemoreceptors of tongue of rat. *J Neurophysiol* **16**, 595–607.
- Bigiani A (2001). Mouse taste cells with gliallike membrane properties. *J Neurophysiol* **85**, 1552–1560.
- Bigiani A (2017). Calcium homeostasis modulator 1-like currents in rat fungiform taste cells expressing amiloride-sensitive sodium currents. *Chem Senses* **42**, 343–359.
- Bigiani A, Cristiani R, Fieni F, Ghiaroni V, Bagnoli P & Pietra P (2002). Postnatal development of membrane excitability in taste cells of the mouse vallate papilla. *J Neurosci* **22**, 493–504.
- Breza JM & Contreras RJ (2012). Anion size modulates salt taste in rats. *J Neurophysiol* **107**, 1632–1648.
- Breza JM, Nikonov AA & Contreras RJ (2010). Response latency to lingual taste stimulation distinguishes neuron types within the geniculate ganglion. *J Neurophysiol* **103**, 1771–1784.
- Bystrova MF, Yatzenko YE, Fedorov IV, Rogachevskaja OA & Kolesnikov SS (2006). P2Y isoforms operative in mouse taste cells. *Cell Tissue Res* **323**, 377–382.
- Caputo A, Caci E, Ferrera L, Pedemonte N, Barsanti C, Sondo E, Pfeffer U, Ravazzolo R, Zegarra-Moran O & Galletta LJ (2008). TMEM16A, a membrane protein associated with calcium-dependent chloride channel activity. *Science* **322**, 590–594.
- Centeio R, Cabrita I, Benedetto R, Talbi K, Ousingsawat J, Schreiber R, Sullivan JK & Kunzelmann K (2020). Pharmacological inhibition and activation of the  $\text{Ca}^{2+}$ -activated  $\text{Cl}^-$  channel TMEM16A. *Int J Mol Sci* **21**, 2557.

- Chandrashekar J, Hoon MA, Ryba NJP & Zuker CS (2006). The receptors and cells for mammalian taste. *Nature* **444**, 288–294.
- Cherkashin AP, Kolesnikova AS, Tarasov MV, Romanov RA, Rogachevskaja OA, Bystrova MF & Kolesnikov SS (2016). Expression of calcium-activated chloride channels Ano1 and Ano2 in mouse taste cells. *Pflugers Arch* **468**, 305–319.
- Clapp TR, Medler KF, Damak S, Margolskee RF & Kinnamon SC (2006). Mouse taste cells with G protein-coupled taste receptors lack voltage-gated calcium channels and SNAP-25. *BMC Biol* **4**, 7.
- Cruz-Rangel S, De Jesús-Pérez JJ, Aréchiga-Figueroa IA, A Rodríguez-Menchaca AA, Pérez-Cornejo P, Hartzell HC & Arreola J (2017). Extracellular protons enable activation of the calcium-dependent chloride channel TMEM16A. *J Physiol* **595**, 1515–1531.
- Dauner K, Lissmann J, Jeridi S, Frings S & Möhrlein F (2012). Expression patterns of anoctamin 1 and anoctamin 2 chloride channels in the mammalian nose. *Cell Tissue Res* **347**, 327–341.
- DeFazio RA, Dvoryanchikov G, Maruyama Y, Kim JW, Pereira E, Roper SD & Chaudhari N (2006). Separate populations of receptor cells and presynaptic cells in mouse taste buds. *J Neurosci* **26**, 3971–3980.
- Dibattista M, Pifferi S, Boccaccio A, Menini A & Reisert J (2017). The long tale of the calcium activated Cl<sup>-</sup> channels in olfactory transduction. *Channels (Austin)* **11**, 399–414.
- Dutta Banik D, Martin LE, Freichel M, Torregrossa A-M & Medler KF (2018). TRPM4 and TRPM5 are both required for normal signaling in taste receptor cells. *Proc Natl Acad Sci U S A* **115**, E772–E781.
- Dvoryanchikov G, Sinclair MS, Perea-Martinez I, Wang T & Chaudhari N (2009). Inward rectifier channel, ROMK, is localized to the apical tips of glial-like cells in mouse taste buds. *J Comp Neurol* **517**, 1–14.
- Ferrera L, Caputo A, Ubbi I, Bussani E, Zegarra-Moran O, Ravazzolo R, Pagani F & Galietta LJV (2009). Regulation of TMEM16A chloride channel properties by alternative splicing. *J Biol Chem* **284**, 33360–33368.
- Henriques T, Agostinelli E, Hernandez-Clavijo A, Maurya DK, Rock JR, Harfe BD, Menini A & Pifferi S (2019). TMEM16A calcium-activated chloride currents in supporting cells of the mouse olfactory epithelium. *J Gen Physiol* **151**, 954–966.
- Herness MS & Sun XD (1999). Characterization of chloride currents and their noradrenergic modulation in rat taste receptor cells. *J Neurophysiol* **82**, 260–271.
- Hisatsune C, Yasumatsu K, Takahashi-Iwanaga H, Ogawa N, Kuroda Y, Yoshida R, Ninomiya Y & Mikoshiba K (2007). Abnormal taste perception in mice lacking the type 3 inositol 1,4,5-trisphosphate receptor. *J Biol Chem* **282**, 37225–37231.
- Huang AY & Wu SY (2018). Substance P as a putative efferent transmitter mediates GABAergic inhibition in mouse taste buds. *Br J Pharmacol* **175**, 1039–1053.
- Huang YA, Maruyama Y & Roper SD (2008). Norepinephrine is coreleased with serotonin in mouse taste buds. *J Neurosci* **28**, 13088–13093.
- Kataoka S, Toyono T, Seta Y & Ogura T & Toyoshima (2004). Expression of P2Y1 receptors in rat taste buds. *Histochem Cell Biol* **121**, 419–426.
- Kim YV, Bobkov YV & Kolesnikov SS (2000). Adenosine triphosphate mobilizes cytosolic calcium and modulates ionic currents in mouse taste receptor cells. *Neurosci Lett* **290**, 165–168.
- Kinnamon SC & Finger TE (2019). Recent advances in taste transduction and signaling. *F1000Res* **8**, 2117, 10.12688/f1000research.21099.1.
- Lawton DM, Furness DN, Lindemann B & Hackney CM (2000). Localization of the glutamate-aspartate transporter, GLAST, in rat taste buds. *Eur J Neurosci* **12**, 3163–3171.
- Liman ER, Zhang YV & Montell C (2014). Peripheral coding of taste. *Neuron* **81**, 984–1000.
- Ma Z, Tanis JE, Taruno A & Foskett JK (2016). Calcium homeostasis modulator (CALHM) ion channels. *Pflugers Arch* **468**, 395–403.
- Ma Z, Taruno A, Ohmoto M, Jyotaki M, Lim JC, Miyazaki H, Niisato N, Marunaka Y, Lee RJ, Hoff H, Payne R, Demuro A, Parker I, Mitchell CH, Henao-Mejia J, Tanis JE, Matsumoto I, Tordoff MG & Foskett JK (2018). CALHM3 is essential for rapid ion channel-mediated purinergic neurotransmission of GPCR-mediated tastes. *Neuron* **98**, 547–561.e10.
- Matsuo R (2000). Role of saliva in the maintenance of taste sensitivity. *Crit Rev Oral Biol Med* **11**, 216–229.
- Maurya DK, Henriques T, Marini M, Pedemonte N, Galietta LJV, Rock JR, Harfe BD & Menini A (2015). Development of the olfactory epithelium and nasal glands in TMEM16A<sup>-/-</sup> and TMEM16A<sup>+/+</sup> mice. *PLoS One* **10**, e0129171.
- Maurya DK & Menini A (2014). Developmental expression of the calcium-activated chloride channels TMEM16A and TMEM16B in the mouse olfactory epithelium. *Dev Neurobiol* **74**, 657–675.
- McBride DW & Roper SD (1991). Ca<sup>2+</sup>-dependent chloride conductance in Necturus taste cells. *J Membr Biol* **124**, 85–93.
- Medler KF, Margolskee RF & Kinnamon SC (2003). Electrophysiological characterization of voltage-gated currents in defined taste cell types of mice. *J Neurosci* **23**, 2608–2617.
- Noguchi T, Ikeda Y, Miyajima M & Yoshii K (2003). Voltage-gated channels involved in taste responses and characterizing taste bud cells in mouse soft palates. *Brain Res* **982**, 241–259.
- Nomura K, Nakanishi M, Ishidate F, Iwata K & Taruno A (2020). All-electrical Ca<sup>2+</sup>-independent signal transduction mediates attractive sodium taste in taste buds. *Neuron* **106**, 816–829.e6.
- O'Driscoll KE, Pipe RA & Britton FC (2011). Increased complexity of Tmem16a/Anoctamin 1 transcript alternative splicing. *BMC Mol Biol* **12**, 35.
- Oliva AA, Jiang M, Lam T, Smith KL & Swann JW (2000). Novel hippocampal interneuronal subtypes identified using transgenic mice that express green fluorescent protein in GABAergic interneurons. *J Neurosci* **20**, 3354–3368.
- Patton C, Thompson S & Epel D (2004). Some precautions in using chelators to buffer metals in biological solutions. *Cell Calcium* **35**, 427–431.



- Pedemonte N & Galietta LJV (2014). Structure and function of TMEM16 proteins (anoctamins). *Physiol Rev* **94**, 419–459.
- Pifferi S, Dibattista M & Menini A (2009a). TMEM16B induces chloride currents activated by calcium in mammalian cells. *Pflugers Arch* **458**, 1023–1038.
- Pifferi S, Dibattista M, Sagheddu C, Boccaccio A, Al Qteishat A, Ghirardi F, Tirindelli R & Menini A (2009b). Calcium-activated chloride currents in olfactory sensory neurons from mice lacking bestrophin-2. *J Physiol* **587**, 4265–4279.
- Pifferi S, Pascarella G, Boccaccio A, Mazzatenta A, Gustincich S, Menini A & Zucchelli S (2006). Bestrophin-2 is a candidate calcium-activated chloride channel involved in olfactory transduction. *Proc Natl Acad Sci U S A* **103**, 12929–12934.
- Ponissery Saidu S, Stephan AB, Talaga AK, Zhao H & Reisert J (2013). Channel properties of the splicing isoforms of the olfactory calcium-activated chloride channel Anoctamin 2. *J Gen Physiol* **141**, 691–703.
- Rock JR, Futtner CR & Harfe BD (2008). The transmembrane protein TMEM16A is required for normal development of the murine trachea. *Dev Biol* **321**, 141–149.
- Roebber JK, Roper SD & Chaudhari N (2019). The role of the anion in salt (NaCl) detection by mouse taste buds. *J Neurosci* **39**, 6224–6232.
- Romanov RA & Kolesnikov SS (2006). Electrophysiologically identified subpopulations of taste bud cells. *Neurosci Lett* **395**, 249–254.
- Romanov RA, Rogachevskaja OA, Bystrova MF, Jiang P, Margolskee RF & Kolesnikov SS (2007). Afferent neurotransmission mediated by hemichannels in mammalian taste cells. *EMBO J* **26**, 657–667.
- Roper SD & Chaudhari N (2017). Taste buds: cells, signals and synapses. *Nat Rev Neurosci* **18**, 485–497.
- Sagheddu C, Boccaccio A, Dibattista M, Montani G, Tirindelli R & Menini A (2010). Calcium concentration jumps reveal dynamic ion selectivity of calcium-activated chloride currents in mouse olfactory sensory neurons and TMEM16b-transfected HEK 293T cells. *J Physiol* **588**, 4189–4204.
- Schroeder BC, Cheng T, Jan YN & Jan LY (2008). Expression cloning of TMEM16A as a calcium-activated chloride channel subunit. *Cell* **134**, 1019–1029.
- Scudieri P, Caci E, Bruno S, Ferrera L, Schiavon M, Sondo E, Tomati V, Gianotti A, Zegarra-Moran O, Pedemonte N, Rea F, Ravazzolo R & Galietta LJV (2012). Association of TMEM16A chloride channel overexpression with airway goblet cell metaplasia. *J Physiol* **590**, 6141–6155.
- Seo Y, Lee HK, Park J, Jeon D-K, Jo S, Jo M & Namkung W (2016). Ani9, a novel potent small-molecule ANO1 inhibitor with negligible effect on ANO2. *PLoS ONE* **11**, e0155771.
- Sinclair MS, Perea-Martinez I, Dvoryanchikov G, Yoshida M, Nishimori K, Roper SD & Chaudhari N (2010). Oxytocin signaling in mouse taste buds. *PLoS One* **5**, e11980.
- Stephan AB, Shum EY, Hirsh S, Cygnar KD, Reisert J & Zhao H (2009). ANO2 is the ciliary calcium-activated chloride channel that may mediate olfactory amplification. *Proc Natl Acad Sci U S A* **106**, 11776–11781.
- Stöhr H, Heisig JB, Benz PM, Schöberl S, Milenkovic VM, Strauss O, Aartsen WM, Wijnholds J, Weber BHF & Schulz HL (2009). TMEM16B, a novel protein with calcium-dependent chloride channel activity, associates with a presynaptic protein complex in photoreceptor terminals. *J Neurosci* **29**, 6809–6818.
- Taruno A, Vingtdoux V, Ohmoto M, Ma Z, Dvoryanchikov G, Li A, Adrien L, Zhao H, Leung S, Abernethy M, Koppel J, Davies P, Civan MM, Chaudhari N, Matsumoto I, Hellekant G, Tordoff MG, Marambaud P & Foskett JK (2013). CALHM1 ion channel mediates purinergic neurotransmission of sweet, bitter and umami tastes. *Nature* **495**, 223–226.
- Taylor R & Roper S (1994). Ca<sup>2+</sup>-dependent Cl<sup>-</sup> conductance in taste cells from *Necturus*. *J Neurophysiol* **72**, 475–478.
- Teng B, Wilson CE, Tu Y-H, Joshi NR, Kinnamon SC & Liman ER (2019). Cellular and neural responses to sour stimuli require the proton channel otop1. *Curr Biol* **29**, 3647–3656.e5.
- Tizzano M, Grigereit L, Shultz N, Clary MS & Finger TE (2015). Immunohistochemical analysis of human vallate taste buds. *Chem Senses* **40**, 655–660.
- Tomchik SM, Berg S, Kim JW, Chaudhari N & Roper SD (2007). Breadth of tuning and taste coding in mammalian taste buds. *J Neurosci* **27**, 10840–10848.
- Tu Y-H, Cooper AJ, Teng B, Chang RB, Artiga DJ, Turner HN, Mulhall EM, Ye W, Smith AD & Liman ER (2018). An evolutionarily conserved gene family encodes proton-selective ion channels. *Science* **359**, 1047–1050.
- Vandenbeuch A, Anderson CB, Parnes J, Enjyoji K, Robson SC, Finger TE & Kinnamon SC (2013). Role of the ectonucleotidase NTPDase2 in taste bud function. *Proc Natl Acad Sci U S A* **110**, 14789–14794.
- Vandenbeuch A, Clapp TR & Kinnamon SC (2008). Amiloride-sensitive channels in type I fungiform taste cells in mouse. *BMC Neurosci* **9**, 1.
- Vandenbeuch A, Zorec R & Kinnamon SC (2010). Capacitance measurements of regulated exocytosis in mouse taste cells. *J Neurosci* **30**, 14695–14701.
- Wladkowski SL, Lin W, McPheeters M, Kinnamon SC & Mierson S (1998). A basolateral chloride conductance in rat lingual epithelium. *J Membr Biol* **164**, 91–101.
- Yang R, Crowley HH, Rock ME & Kinnamon JC (2000). Taste cells with synapses in rat circumvallate papillae display SNAP-25-like immunoreactivity. *J Comp Neurol* **424**, 205–215.
- Yang R, Dzowo YK, Wilson CE, Russell RL, Kidd GJ, Salcedo E, Lasher RS, Kinnamon JC & Finger TE (2020). Three-dimensional reconstructions of mouse circumvallate taste buds using serial blockface scanning electron microscopy: I. Cell types and the apical region of the taste bud. *J Comp Neurol* **528**, 756–771.
- Yang YD, Cho H, Koo JY, Tak MH, Cho Y, Shim W-S, Park SP, Lee J, Lee B, Kim B-M, Raouf R, Shin YK & Oh U (2008). TMEM16A confers receptor-activated calcium-dependent chloride conductance. *Nature* **455**, 1210–1215.

- Ye W, Chang RB, Bushman JD, Tu Y-H, Mulhall EM, Wilson CE, Cooper AJ, Chick WS, Hill-Eubanks DC, Nelson MT, Kinnamon SC & Liman ER (2016). The K<sup>+</sup> channel KIR2.1 functions in tandem with proton influx to mediate sour taste transduction. *Proc Natl Acad Sci U S A* **113**, E229–E238.
- Yunos NM, Bellomo R, Story D & Kellum J (2010). Bench-to-bedside review: chloride in critical illness. *Critical Care* **14**, 226.
- Zhang Y, Hoon MA, Chandrashekar J, Mueller KL, Cook B, Wu D, Zuker CS & Ryba NJP (2003). Coding of sweet, bitter, and umami tastes: different receptor cells sharing similar signaling pathways. *Cell* **112**, 293–301.
- Zhang Y, Zhang Z, Xiao S, Tien J, Le S, Le T, Jan LY & Yang H (2017). Inferior olivary TMEM16B mediates cerebellar motor learning. *Neuron* **95**, 1103–1111.e4.

## Additional information

### Data availability statement

The data that support the findings of this study are available from the corresponding author upon reasonable request. The peer review history is available in the Supporting Information section of this article.

### Author contributions

D.M.G., K.Y.G.-V. and A.H.-C. designed and performed the research, and analysed the data. A.M. and S.P. designed the research, analysed the data and wrote the paper.

### Competing interests

The authors declare no conflicts of interests

### Funding

This work was funded by the Italian Ministry of Education, University and Research 2010599KBR (A.M.).

### Acknowledgements

We thank Michele Dibattista (University of Bari) and Paul A. Heppenstall (SISSA) for helpful discussions. We thank Elettra Grdina, Angel Pascual Camerota, Cristina Degrassi, Lorenzo Maschietto and Giovanni Tamburin for mice handling, and Helena Krmac and Christina Vlachouli for mice genotyping. We thank Lily Jan (UCSF), Jason R. Rock (Boston University School of Medicine) and Brain D. Harfe (University of Florida) for providing the KO mice.

### Keywords

ANO1, anoctamin 1, taste bud

### Supporting information

Additional supporting information can be found online in the Supporting Information section at the end of the HTML view of the article. Supporting information files available:

### Peer Review History Statistical Summary Document